2021

Relating Streamflow Discharge to Surface Elastic Response Under Hydrologic Loading Using Single GPS Vertical Displacement and the Storage-Discharge Relationship at Local Watershed Scales

Noah B. Clayton
University of Montana, Missoula

Relating Streamflow Discharge to Surface Elastic Response Under Hydrologic Loading Using Single GPS Vertical Displacement and the Storage-Discharge Relationship at Local Watershed Scales

By

Noah Clayton

A thesis submitted in partial satisfaction of the requirements for the degree of

M.S. in Geosciences

in the

Department of Geosciences

at the

University of Montana

Committee:

Dr. W. Payton Gardner, University of Montana, Missoula, MT

Dr. Hilary Martens, University of Montana, Missoula, MT

Dr. Adrian Borsa, Scripps Institution of Oceanography, San Diego, CA

January 2022

Abstract. Uncertainties associated with climate change and increasing demands for water resources require better methods for estimating water availability at small to intermediate watershed scales (<1500 km^2). Temporal changes in watershed storage and transport across various watersheds in the western U.S. were investigated using the hydrologic loading signal from GPS vertical displacements as a proxy for changes in watershed total terrestrial storage. GPS vertical displacement and streamflow discharge relationships were analyzed at daily to monthly temporal resolution. Stream connected storage changes were inferred using discharge using a first-order dynamical system model. Storage inferred from discharge, GPS vertical displacement and storage inferred from a regional scale western U.S. GPS network array were compared. Analyzing the average behavior over the period of record (10+ years), we find that GPS vertical displacement is well correlated to discharge during periods of hydrograph recession resulting in R^2 values ranging from (0.78 to 0.96) with 30-day smoothing. We show that local GPS measurements are in close agreement with regional GPS storage inferences. When GPS station array density is sparse, local GPS stations display better agreement with discharge inferred storage estimates and have the potential to provide higher spatial and temporal resolution relative to current published methods of inferring storage from regional GPS inversions. The GPS vertical displacement-discharge relationship provides an independent analysis of watershed function, insight into antecedent conditions, and strong correlations that may enhance predictive power when estimating water availability at local watershed scales most useful to hydrologist and water resources management.

1. Introduction

Consumptive demands of water resources are rapidly increasing while surface and groundwater reservoirs are decreasing at rates faster than they can be naturally replenished (e.g., Yager, 2019). Increasing evidence supports the intensification of the hydrological cycle in response to global climate warming (e.g., Donat et al., 2016). Hydrologic events such as drought or flooding (e.g., Meixner, 2016) are extremely sensitive to climate change and hold great concern for water resources management. Much of the arid to semi-arid regions across the western U.S. rely on seasonal delivery of precipitation (e.g., Meixner, 2016), in the form of rain or snowpack, providing critical annual water supplies to ecosystems, communities, and agricultural interests. Optimal use and management of these resources requires improving our ability to track, measure, and estimate water availability. The elastic response of Earth's surface under seasonal hydrologic loads, as recorded by vertical displacements from the network of the Americas (NOTA) western U.S. array of global positioning systems, have provided insight into changes in terrestrial water storage across the landscape at large regional scales (Argus, 2014; 2017, Borsa et al., 2014, Fu et al., 2015). Improvement upon these methods is required to increase spatial and temporal resolution of GPS displacement as an operational tool in hydrology at small to intermediate watershed scales to provide utility for hydrologists and water resources management.

The lithosphere responds elastically to mass loading (Farrell, 1972). Atmospheric transport of oceanic and freshwater masses inflicts variable surface pressures ranging from hours to interannual timescales (e.g., Argus et al., 2014; 2017; Borsa et al, 2014; Birhanu and Bendick 2015; Fu et al., 2015; Martens et al., 2016). Seasonal surface loads, caused by hydrologic loading, are the primary driver of annual displacement and manifest in the geodetic signal as a

downward response as the load is applied and upward rebound as the load is removed (Heki, 2001; van Dam et al., 2001; Dong et al., 2002).

Snowpack is an important contributor to annual water resources in the western U.S. (eg., Barnett et al., 2005; Earman et al., 2006). GPS studies have shown strong inverse correlation between seasonal geodetic displacement and snow water equivalent (SWE) under seasonal snowpack loading (e.g., Heki et al., 2001; Ouellette et al., 2013). GPS stations and SNOTEL sites located in close proximity (10's of km) display the strongest relationships between SWE and GPS vertical displacement (Knappe et al., 2019). Elevations receiving snow loads show snowpack and soil moisture dominate the seasonal geodetic signal at mountain sites in the western U.S. (e.g., Ouellette et al., 2013) but fail to accurately predict SWE from an inability to accurately partition the SWE signal from soil moisture or other hydrologic loads as measured by GPS surface displacement.

Precise GPS measurements over long and continuous time series from the NOTA array of 1276+ GPS stations across the western U.S. have been filtered and processed to isolate hydrologic responses in the GPS/GNSS signal. The isolated hydrologic signal has been inverted using Green's functions to infer regional GPS inferred storage changes (RGPSS) over large regions of the western U.S. (Argus et al., 2017; Borsa et al., 2014). Riegger and Tourian (2014) employed a method to infer changes in storage and discharge from GRACE mass change determinations at the global or large regional scale (≈ 300+ km). RGPSS methods show agreement with regional GRACE inferences of changes in water thickness, suggesting potential to bridge the scaling gap between 300 km^2 GRACE and point source observations of hydrologic storage and loading from traditional hydrologic measurments (Argus et al., 2014, Borsa et al., 2014, Fu et al., 2015).

To date, double differencing methods utilize measurements from large arrays of GPS/GNSS to increase accuracy in precision of the GPS/GNSS position estimate (eg., Borsa et al., 2014) which are required to invert signals using Green's function (Argus et al.,2014). However, most published storage estimates are monthly averages at a relatively course spatial resolution (100's – 1000's km). Current methods lack the spatial and temporal resolution often required by hydrologists or water resources managers to accurately estimate water availability at intermediate to local watershed scales (10's – 100's km). Recently, new methods to establish and remove regional trends from GPS network signals (Knappe et al., 2019) show the potential of GPS to fill the spatial gap between measuring intermediate watershed scale vertical GPS displacement and GRACE/regional GPS vertical displacement under hydrologic loading. These results indicate that GPS vertical displacement could be useful for meauring watershed storage states.

Bevis et al., (2005) estimated seasonal fluctuations in surface water mass over the central Amazon basin from a single GPS station and found strong anti-correlation with the local stage height of the Amazon River. The results indicate that a single GPS can be strongly and inversely correlated to discharge and storage in large basins within ~200 km of the GPS measurement. However, with such a large basin, the individual measurement was unable to detect individual precipitation events. Steckler et al. (2010) used stream stage height, GPS, and GRACE data to estimate both solid earth elastic properties and storage changes due to monsoonal flooding in Bangladesh. These estimates relied heavily on porosity assumptions, manual stage height data collection, and GRACE to infer loading from storage in a complex, large, and geologically active area with close agreement between the two GPS stations and GRACE measurements. To date, the relationship between discharge and surface deflection has not been thoroughly

examined at the small to intermediate watershed scale using single GPS station vertical displacement (GPSVD) measurements.

In this paper, we investigate the potential of GPSVD as a proxy measurement for local watershed storage to constrain the storage-discharge relationship. We use GPSVD to investigate watershed storage and discharge dynamics. We observe a strong response of the individual GPS measurement to seasonal changes in hydrologic loading, identify functions of watershed storage and transport through GPSVD-discharge relationships, and identify periods when GPSVD and discharge are well correlated. We show that GPSVD can provide insight into the storage-discharge relationship and offers predictive enhancement of water availability at local watershed scales with increased temporal resolution (daily to monthly) in a variety of small catchments across the western U.S.

2. Study Locations

Watersheds of interest were selected based on the following criteria: Western U.S. watersheds located at the headwaters of streams and receiving substantial seasonal precipitation; with a NOTA GPS station within (or close proximity to) the watershed and an existing USGS streamflow gauge. Watersheds of interest were limited to sites where discharge and geodetic data contained, at minimum, 10 years of consistent time-series data. We employ several publicly available data sets including GPS time series from UNAVCO (www.unavco.org), USGS streamflow time-series (www.waterwatch.usgs.gov) for streamflow discharge, SNOTEL time-series (www.nrcs.usda.gov) for point source snow water equivalent measurements (SWE), and gridded precipitation time-series from gridMET (http://thredds.northwestknowledge.net:8080/thredds/reacch_climate_MET_aggregated_catalog.html). We selected 2 snowpack-dominated and 3 rain-dominated watersheds fitting these criteria (Figure 1). Snow dominant watersheds include the seasonally dry Camas Creek (CC) located in the Northern Rockies of Idaho and the summer monsoonal watershed of Roaring Fork River watershed (RFR) in the central Rocky Mountains of western Colorado, the largest watershed (3763 km^2) in the study. We investigate the entire Roaring Fork River watershed using GPS station P728 along with two sub-watersheds, the upper Roaring Rork River (RFRU) (≈275 km^2) and the Crystal River (RFRC) (≈433 km^2). Camus Creek is located on Camas Prarie in southern Idaho and covers ~1621 km^2. In Camus Creek watershed, two GPS sites (P350 and P019) were used and one stream gauge at the watershed outlet. Selected rain dominant watersheds include the Russian River and the N.Yuba River (NYUBA) in California. In the Russian River, we focused on two headwater sub-basins: the West Fork of the Russian River (WFRR) (~259 km^2), using GPS station P190 and the East Fork of the Russian River (EFRR) (~239 km^2) using GPS P192 in Potter Valley, CA. The North Yuba (≈ 648 km^2) is located in the low Sierra Mountains (GPS station P144) and briefly receives some snow in winter. We will refer to North Yuba further as a transitional watershed, but we consider it predominantly a rain-dominated watershed.

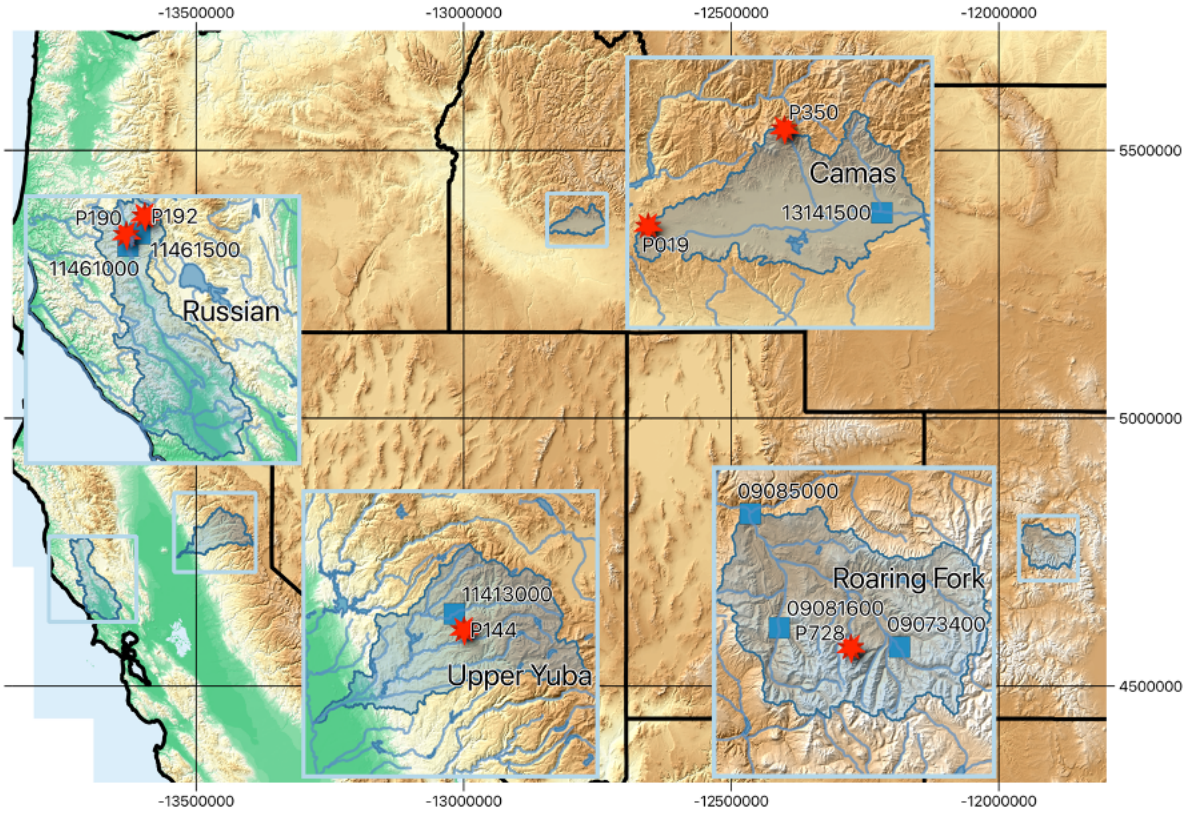

Figure 1: Map of study watersheds in western U.S.

2. *Methods*

Watershed Storage:

Understanding how a watershed functions is critical for estimating water availability and watershed hydrologic response to forcings. Transport and storage are essential watershed functions unique to each watershed. In high mountain ranges, snowpack accumulates and is stored until the arrival of spring and warming temperatures. In rain-dominated watersheds, seasonal precipitation saturates the landscape recharging surface waters, soil moisture, aquifers, deep groundwater systems, and supplies streamflow essential for downstream ecosystems and communities. Terrestrial water storage (storage) encompasses all water in a watershed including snowpack, surface waters, water in the biosphere, soil moisture, and groundwater systems. The amount of storage in a watershed is continually changing at rates governed by intrinsic characteristics such as topography, vegetation, lithology, geologic structure, and climate unique to each watershed. The area normalized terrestrial water budget for a watershed is summarized as:

$$\frac{dS}{dt} = P - ET - Q \quad (1)$$

where (S) represents storage (L) in the watershed, (P) precipitation (L/t), (ET) evapotranspiration (L/t), (Q) discharge (L/t). Precipitation is the only input in equation (1), which is then partitioned into storage, or exits the watershed via ET or discharge (Q). ET measurements are difficult to accurately estimate due to spatiotemporal variability in rates of storage loss through evaporation from soil and transpiration from a wide variety of vegetation types (eg., Woodward, 1987; Neilson, 1995). Historically, changes in storage have proven difficult to estimate due to high spatial and temporal heterogeneity of the surface and subsurface properties, ET and P. In practice, when estimating water availability, only P and Q are measured leaving both S and ET as unknowns in the watershed budget (equation 1).

Changes in storage in a watershed are dependent on catchment sensitivity to climatic forcing (Berghuijs et al., 2016). This sensitivity comes from the watershed characteristics that cause the temporal disparities between hydrologic inputs and consequent streamflow discharge responses (Kirchner, 2009; Botter, 2009). Antecedent wetness conditions impact watershed sensitivity as expressed in wide ranging runoff coefficients with orders of magnitude difference even when given equal magnitudes of precipitation (Tromp-van Meerveld and McDonnell, 2006).

Hydrologically coupled storage (e.g., groundwater aquifers) directly influence discharge whereas uncoupled storage (e.g., snowpack, surface ponding) does not directly lead to discharge due to temporal delays, removal by evaporation, or exportation via regional groundwater flow paths (e.g., Riegger and Tourian, 2014). Partitioning between coupled and uncoupled storage and the relationship between coupled storage and discharge in complex terrain continues to be a fundamental pursuit in hydrologic studies (e.g., Maxwell et al., 2016). Each watershed has unique characteristics governing residence and transport times as water navigates down gradient to expresses itself in streams. Late season flows are maintained by these gradual groundwater releases along the length of the stream. A well adopted theme in catchment hydrology is that discharge is related to coupled storage (e.g., Horton, 1936; 1937; 1941; Brutsaert and Nieber, 1977; Kirchner, 2009). Basin-scale hydraulic properties can be interpreted through hydrograph recession curve analysis (Brutsaert and Nieber, 1977, Brutsaert and Lopez, 1998) providing the opportunity to infer changes in watershed storage (equation 1) when P and ET are minimized providing discharge as a function of storage alone thus, directly yielding a close approximation of storage (Kirchner, 2009).

Data Acquisition, and Processing:

In this study, we employ GPSVD as a proxy measurement for watershed storage. We processed UNAVCO mean daily vertical displacement (mm) time series from continuous GPS provided in IGS14 reference frame made publicly available by UNAVCO (www.unavco.org) to isolate GPS vertical displacement due to hydrologic loading. To account for offsets due to earthquakes, we used UNAVCO's offset locations (Herring et al., 2016), removed a harmonic with annual and semi-annual terms, and fit a linear trend to 60 days before and after the offset event using daily uncertainties as weights and amplitude equaling the day before minus the first day of the linear trend, and corrected the time series using a unit step function. To isolate the hydrologic geodetic signal, we fit a linear trend to the offset-corrected GPS time series to remove any regional tectonic activity in the signal. Next, we remove non-tidal atmospheric loading (and non-tidal oceanic loading data using ESMGFZ Surface Loading Products (Dill, R. and H. Dobslaw, 2013) (http://rz-vm115.gfz-potsdam.de:8080/repository). We follow (Klos et al., 2015) to identify and remove outliers relative to the median absolute deviation modified by using a

rolling 120-day window to calculate periods 60 days before and after the outlier event, then calculate the median, median absolute deviation, and standard deviation before moving to the next day resulting in a time varying median, median absolute deviation, and standard deviation. To this standard deviation, we apply a factor of 1.4826 converting the median absolute deviation to its equivalent Gaussian robust standard deviation (Klos et al. 2015). Any GPS positions in the original time series more than 3 Gaussian standard deviations over the 120-day window were removed.

Intantaneous stream discharge in ft^3/s data was obtained from USGS (waterwatch.usgs.gov) in 15-minute intervals for the period of study. Instaneous discharge was converted to (m^3/s) and then binned by day to calculate mean daily discharge (m^3/d). Volumetric discharge was normalized by the watershed area provided by USGS to convert to runoff (mm/d) to provide a similar unit of measurement (mm/d) for GPSVD and for which watershed storage is measured.

We use gridded monthly Regional GPS inferred Storage storage (RGPSS) (mm/month) after Argus et al. (2017), spanning January 1, 2006 through September 2020. These storage estimates are inferred by inverting an elastic deformation model against observed hydrologic load vertical displacements from a large network of existing GPS stations across the western U.S. The elastic model employs Greens Functions for a gravitating, spherical, stratified Earth for PREM (Wang et al., 2012) at 1/8° intervals of latitude and longitude. The data set used for inversion has GPS sites exhibiting a poroelastic response to groundwater changes and sites with volcanic activity removed. For the remaining sites vertical displacements associated with atmospheric loading, glacial isostatic adjustment, and changes from artificial reservoirs were removed (Argus et al. 2017). We used the mean monthly storage value from RGPSS gridded data from the single closest pixel to each GPS station located in our study watersheds.

SNOTEL stations were used for point measurements of Snow Water Equivalent (SWE) and temperature in snow dominated watersheds (https://www.wccnrcs.usda.gov/snow). SNOTEL sites record hourly measurements of SWE using a snow pillow to an accuracy of 0.254 mm. For this study, we use daily SNOTEL estimates for accumulated SWE (mm/d) and average daily temperature (°C).

High spatial resolution (~4 km), daily gridded surface precipitation was obtained from GRIDMET (Abatzoglou, 2012). The dataset blends the high-resolution spatial data from PRISM with the high temporal resolution data form the National Land Data Assimilation System (NLDAS) model using climatically aided interpolation to produce spatially and temporally complete gridded dataset of surface meteorological variables. Daily total precipitation consists of the sum of all forms of precipitation summed and converted to a water-equivalent measurement. GRIDMET data was clipped to shapefiles for each watershed and daily values of precipitation (mm/d) were averaged for all grids within the watershed boundaries.

For both GPSVD and discharge, kernel smoothing was performed using a (1,3, 7 14, and 30-day) rolling weighted average. To obtain the average behavior of discharge, precipitation, SWE, and GPSVD in each of our study watersheds, we calculate the average value for each calendar day over the period of record (POR) for each watershed. POR was limited by GPS time series availability. Water years begin on October 1st and end on September 30th of each year. We converted standard calendar days to days of water year (Oct.1 = day 1 and September 30th = day 365, and leap year days (366) were omitted).

Discharge Derived Storage:

Following Kirchner (2009), we use raw and smoothed daily discharge values to infer stream connected storage, which we will refer to as Discharge Inferred Storage (DIS). When precipitation and evapotranspiration are minimal (Equation 1), discharge (Q) is a monotonic function of storage (S) and is described by the following storage-discharge relationship:

$$Q = f(S)$$

allowing for direct inference of storage by integrating discharge (Kirchner, 2009):

$$\int dS = \int \frac{dQ}{g(Q)} \tag{2}$$

where $g(Q) = dQ/dS$ is the implicit differential form of the storage-discharge relationship expressing sensitivity to changes in storage as a function of discharge and unique to each watershed. There are competing methods to identify the sensitivity function from streamflow recession analysis, a linear model (e.g. Kirchner, 2009) and a non-linear model (e.g. Botter, 2009). The non-linear form accounts for the random nature of rainfall using a stochastic mass balance framework to derive the statistical distribution and the duration curve of stream flows (Botter, 2009). The linear form uses the central tendency of recession flow data (Kirchner, 2009). Riegger and Tourian (2014) show that the non-linear form can be fully assigned to uncoupled storage (which do not directly lead to impacts in discharge) and coupled storage (directly related to discharge) takes on the linear sensitivity function. We adopt Kirchner's (2009) method employing the following sensitivity function for periods during hydrograph recession when conditions meet requirements (Equation 1) of (P,ET << Q):

$$g(Q) = \frac{dQ}{dS} = \frac{{}^{dQ}/_{dt}}{{}^{dS}/_{dt}} = \frac{{}^{dQ}/_{dt}}{-Q} \tag{3}$$

For storage-discharge analysis and interpretation, we follow a multitude of others (e.g., Brutsaert and Nieber, 1977; Kirchner, 2009) to best fit the discharge rate of change by parameterizing a power law function uniquely describing the rate of discharge as a function of discharge in each watershed:

$$-\frac{dQ}{dt} = \alpha Q^{\beta} \tag{4}$$

Following Kirchner (2009), we adhere to hydrograph recession analysis periods where P, ET << Q by filtering out discharge data when precipitation events were within one order of magnituge of the concurrent discharge measurement and if precipitation occurred less than 24 hours prior to discharge measurement. ET is minimized in mid-late season hydrograph recession when water limited conditions exist at shallow soil depths (eg., Woodward, 1987; Neilson,

1995). To further minimize the effects of ET, we used 15-minute interval non-smoothed discharge rates ($-\frac{dQ}{dt}$) and binned hourly averages between midnight and 4:00 a.m. and performed log-log analysis of $-\frac{dQ}{dt}\ vs.\ Q$. Combining equations 2,3, and 4 we get:

$$\int dS = \int \frac{1}{a}\ Q^{1-\beta}\ dQ \tag{5}$$

Which can be integrated to give:

$$S - S_o = \frac{1}{\alpha}\ \frac{1}{2-\beta}\ Q^{2-\beta} \tag{6}$$

where S is storage, S_o is the constant of integration (here, the mean value of inferred storage for the period of study), and Q is discharge (Kirchner, 2009). Watershed specific parameters for (4) were determined by fitting appropriately filtered observed Q and dQ/dt in each watershed. The fitted parameters characterize a watershed's unique storage-discharge behavior and were substituted into equation (6) to infer stream connected storage in the watershed from discharge:

Statistical Metrics:

With processed data values, we normalized GPSVD, discharge, RGPSS, and DIS estimates for comparison using the following equation:

$$x = \frac{x_i - x_{min}}{x_{max} - x_{min}}$$

where x_i is the value being normalized. Next, we perform correlation analysis using Pearson product-moment correlation coefficients in which the correlation coefficient matrix, R, and covariance matrix, C, is:

$$R_{ij} = \frac{C_{ij}}{\sqrt{C_{ii} * C_{jj}}}$$

to determine all correlation coefficients between GPS vertical measurements to discharge, storage estimates obtained from RGPSS, and DIS. This correlation coefficient is squared to obtain R^2 values.

3. Results

Qualitative analysis between discharge and GPSVD:

3-day weighted average time series of discharge and GPSVD plotted against water years (Figure 2.1 – 2.3) display a seasonally consistent inverse relationship between GPSVD and discharge. As GPSVD moves downward discharge increases and conversely, when GPSVD moves upward discharge is decreasing. GPSVD maximums align with water year boundaries when discharge is at minimums for each water year. The exception is observed in Roaring Fork

River watersheds (Figure 2.2: a, b, and c) where recession continues through winter months and minimum discharge occurs near maximum negative GPSVD before rebounding occurs. In rain-dominated watersheds (Figure 2.3: a,b, and c) GPSVD minimums (maximum downward displacements) occur near peak discharge. We note an exception to this behavior in WFRR and EFRR in water years 2011 and 2017 (Figure 2.3: a and b), where GPSVD lags peak discharge, whereas snow-dominated watersheds exhibit some lag between GPSVD minimums and discharge maximums where peak discharge occurs later in the water year relative to rain-dominated watersheds. The lag is consistent and especially noticeable in Roaring Fork River watersheds.

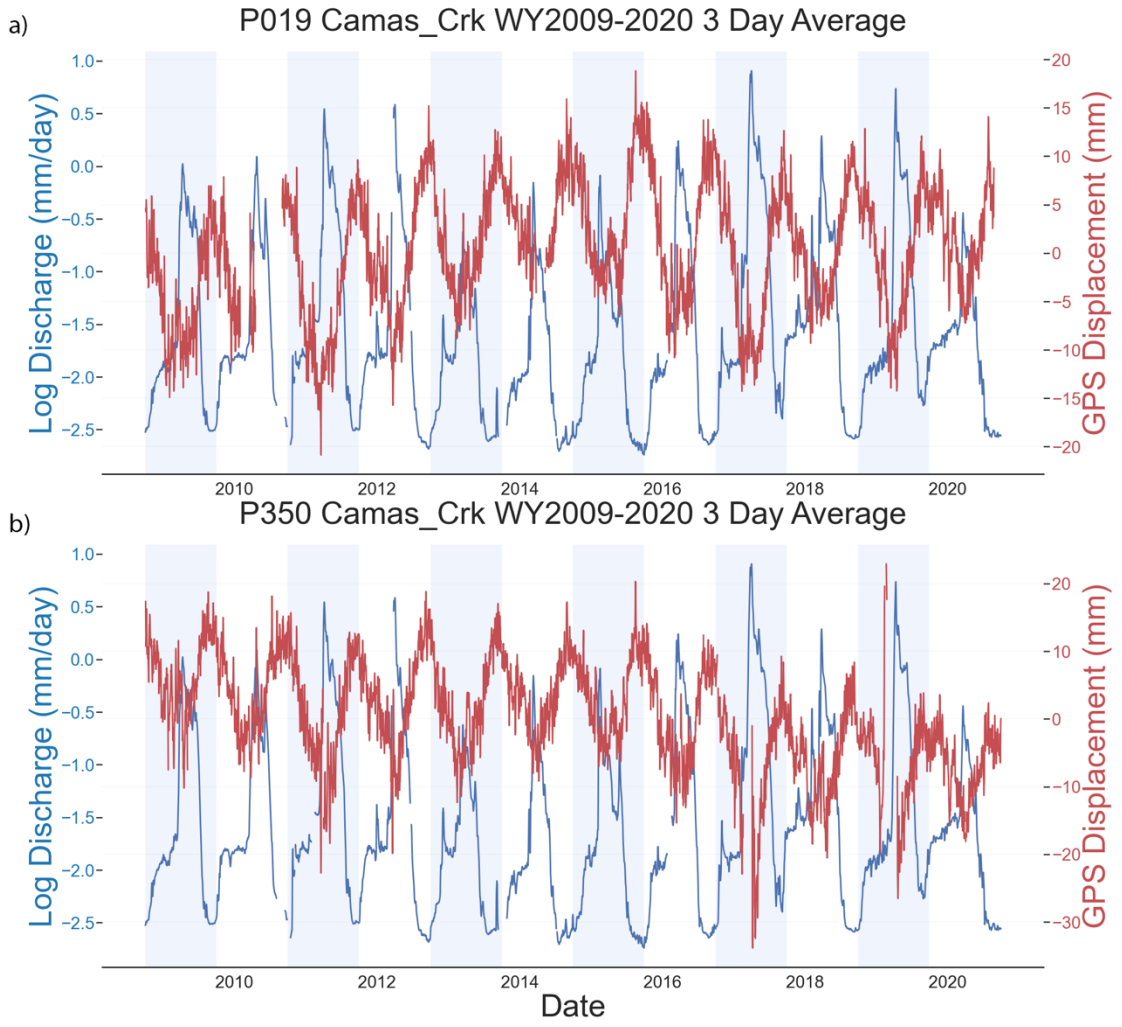

Figure 2.1: Time Series for CC P019 (a) and CC P350 (b) of 3-day rolling weighted averages of discharge (blue) and GPS (red) plotted against water years of study in Camas Creek. Water years are delineated by light blue and white background bars where blue meets white at the start (Oct.1st) and end (Sept.30th) of each water year. GPSVD values follow standard geodetic convention here where negative values represent downward GPSVD under hydrologic loading and positive direction values represent surface rebound.

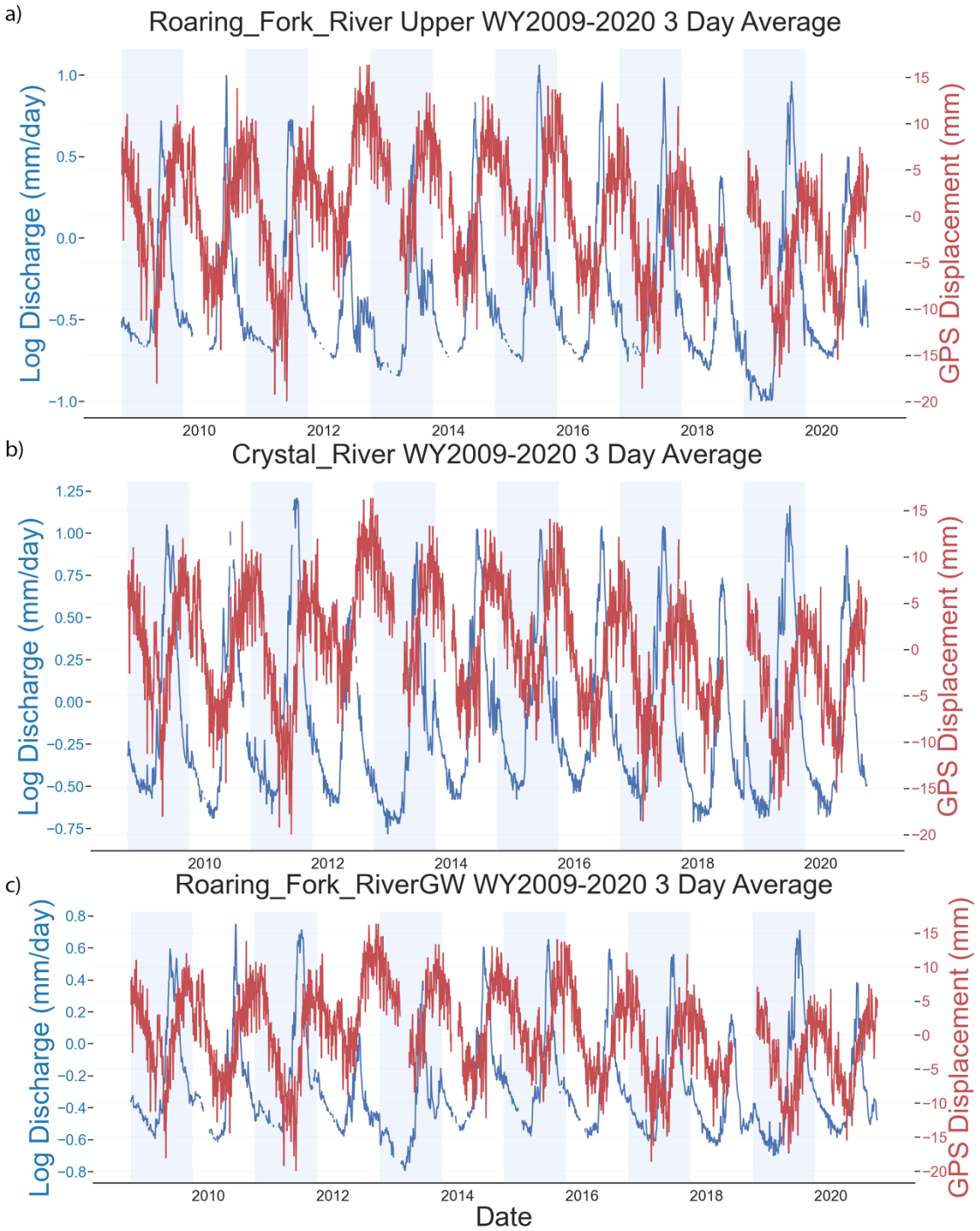

Figure 2.2: Time Series for RFRU (a), RFRC (b), and RFR (c) of 3-day rolling weighted averages of discharge (blue) and GPS (red) plotted against water years of study in the Roaring Fork watershed. Water years are delineated by light blue and white background bars where blue meets white at the start (Oct.1st) and end (Sept.30th) of each water year. GPSVD values follow standard geodetic convention here where negative values represent downward GPSVD under hydrologic loading and positive direction values represent surface rebound.

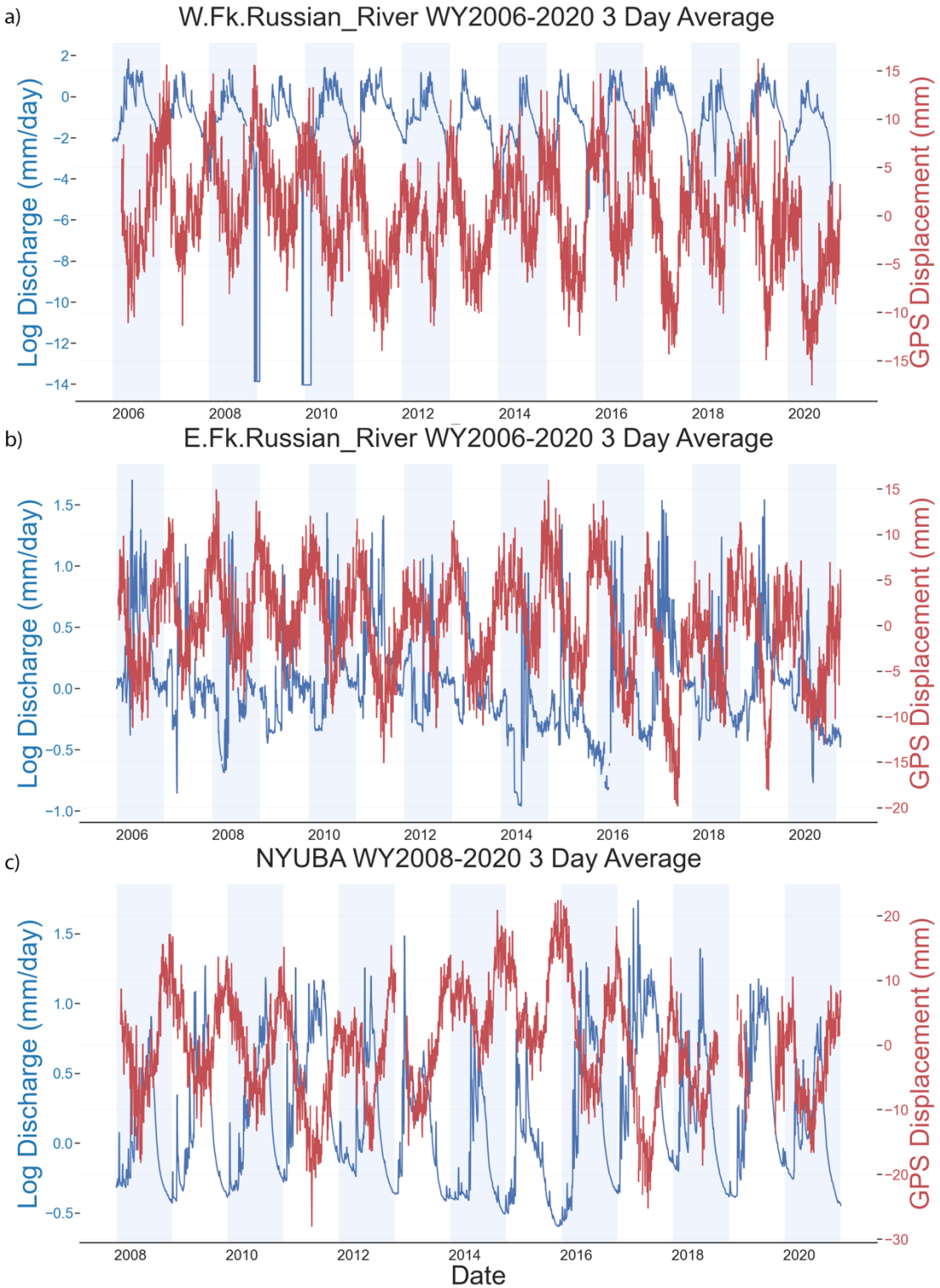

Figure 2.3: Time Series for WFRR (a) and EFRR (b) and NYUBA (c) of 3-day rolling weighted averages of discharge (blue) and GPS (red) plotted against water years of study for transitional (c) and rain dominant (a & b) watersheds. Water years are delineated by light blue and white background bars where blue meets white at the start (Oct.1st) and end (Sept.30th) of each water year. GPSVD values follow standard geodetic convention here where negative values represent downward GPSVD under hydrologic loading and positive direction values represent surface rebound.

Qualitative analysis of average GPSVD response to hydrologic processes:

We observe a strong response in average response of GPSVD to hydrologic signals of SWE and precipitation (Figures 3.1 - 3.3). Again, we observe a consistent and strong inverse relationship between GPSVD and observed discharge, especially during periods of hydrograph recession. GPSVD moves downward with the rising limb of discharge in rain-dominated watersheds where discharge builds and plateaus through the wet season, early to mid-water year, reaching maximum GPSVD at the end of the wet season. In snow-dominated watersheds GPSVD downward response is dominated by SWE reaching maximum displacement when maximum snowpack accumulation occurs. In Camas Creek, GPSVD rebound occurs after SWE accumulation disappears whereas in Roaring Fork watersheds, rebound occurs with the onset of the melt season. As precipitation subsides and/or snowpack disappears, hydrograph recession occurs and subsequent rebound of GPSVD is observed in all watersheds.

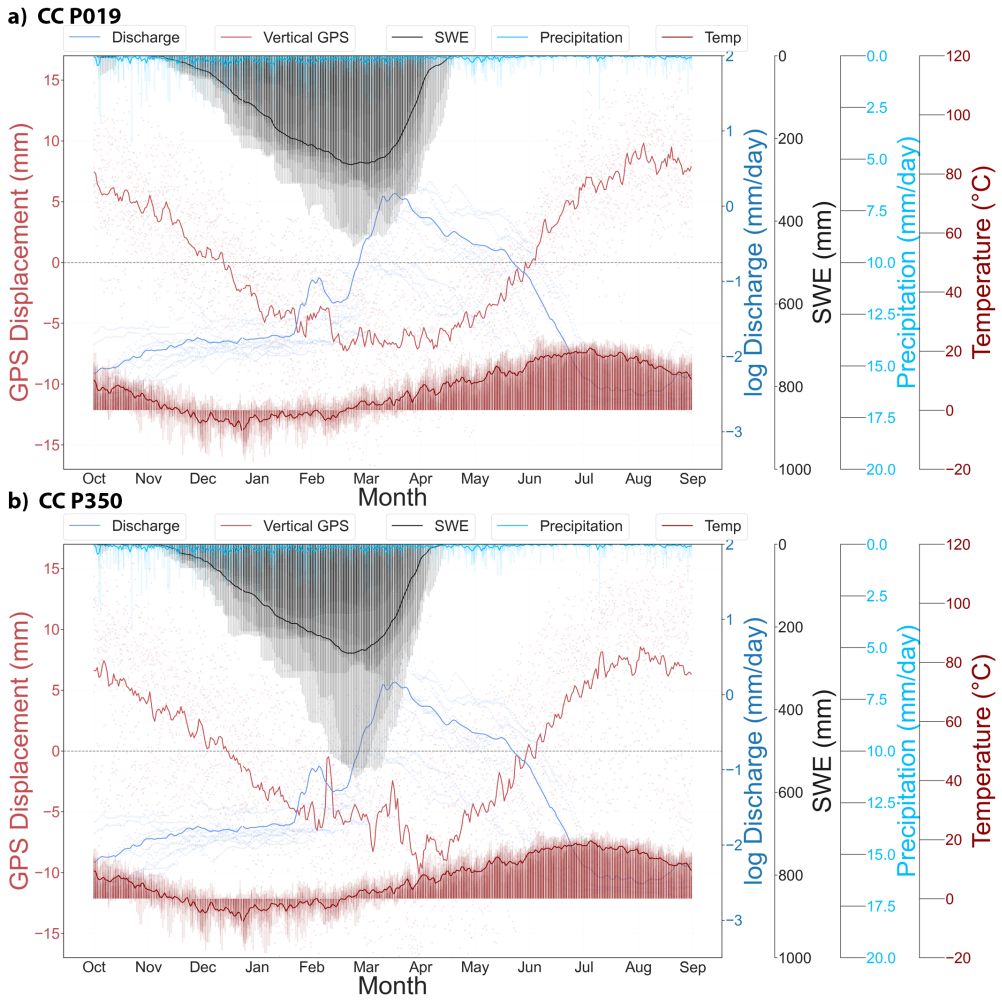

Figure 3.1: 3-day smoothed time series for CC P019 (a) and CC P350 (b) of average daily values (solid lines) for GPSVD in Camas Creek watershed. GPSVD is plotted (in red), log discharge (in dark blue), precipitation from GRIDMET (light blue), SWE (black), and temperature (reddish brown) from which SNOTEL). Daily values for individual years are plotted at reduced opacity. Horizontal axis displays the month of the water year beginning October 1st and ending on September 30th.

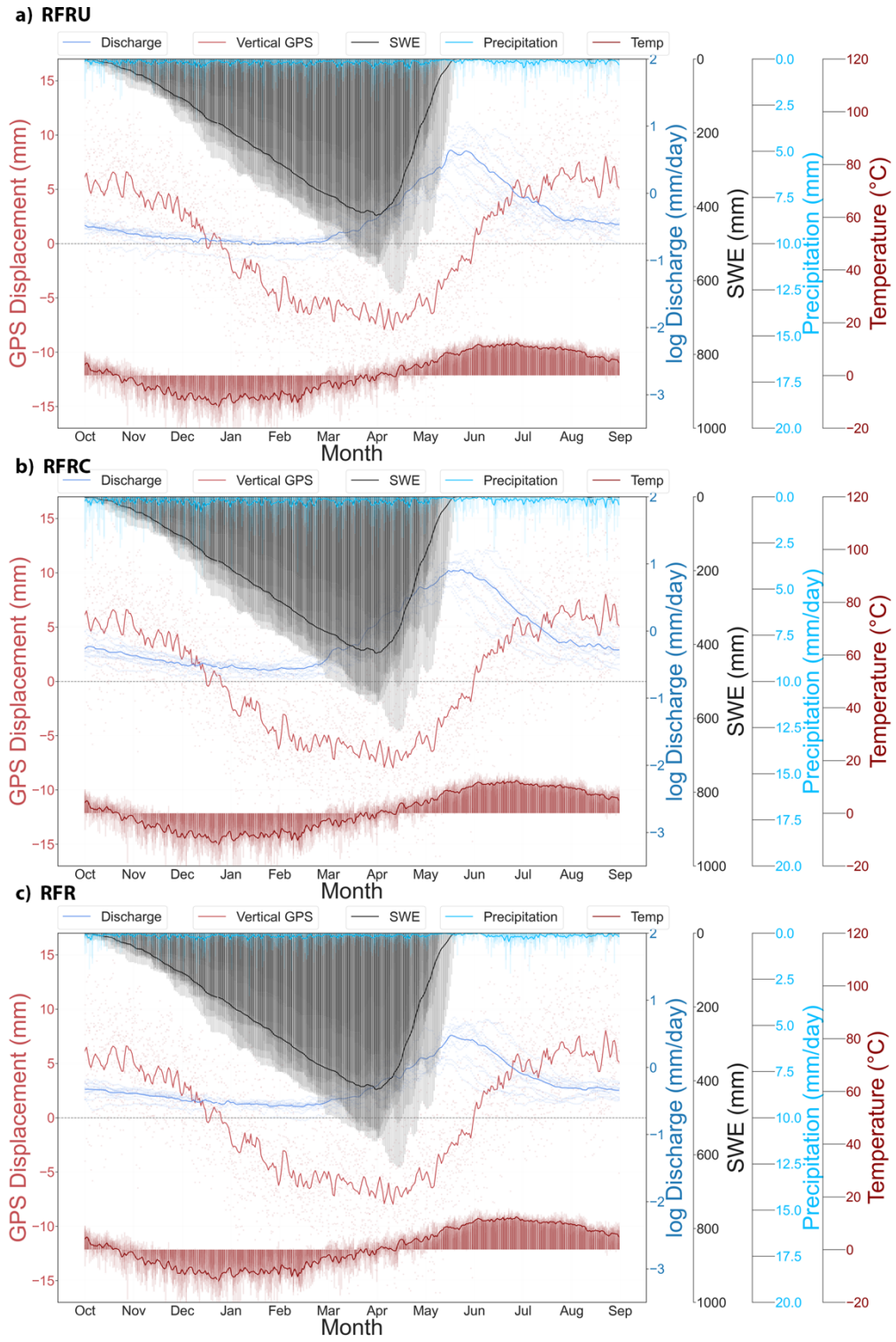

Figure 3.2: 3-day weighted average time series for RFRU (a), RFRC (b), and RFR (c) of average daily values (solid lines) for GPSVD in Camas Creek watershed. GPSVD is plotted (in red), log discharge (in dark blue), precipitation from GRIDMET (light blue), SWE (black), and temperature (reddish brown) from which SNOTEL). Daily values for individual years are plotted at reduced opacity. Horizontal axis displays the month of the water year beginning October 1st and ending on September 30th.

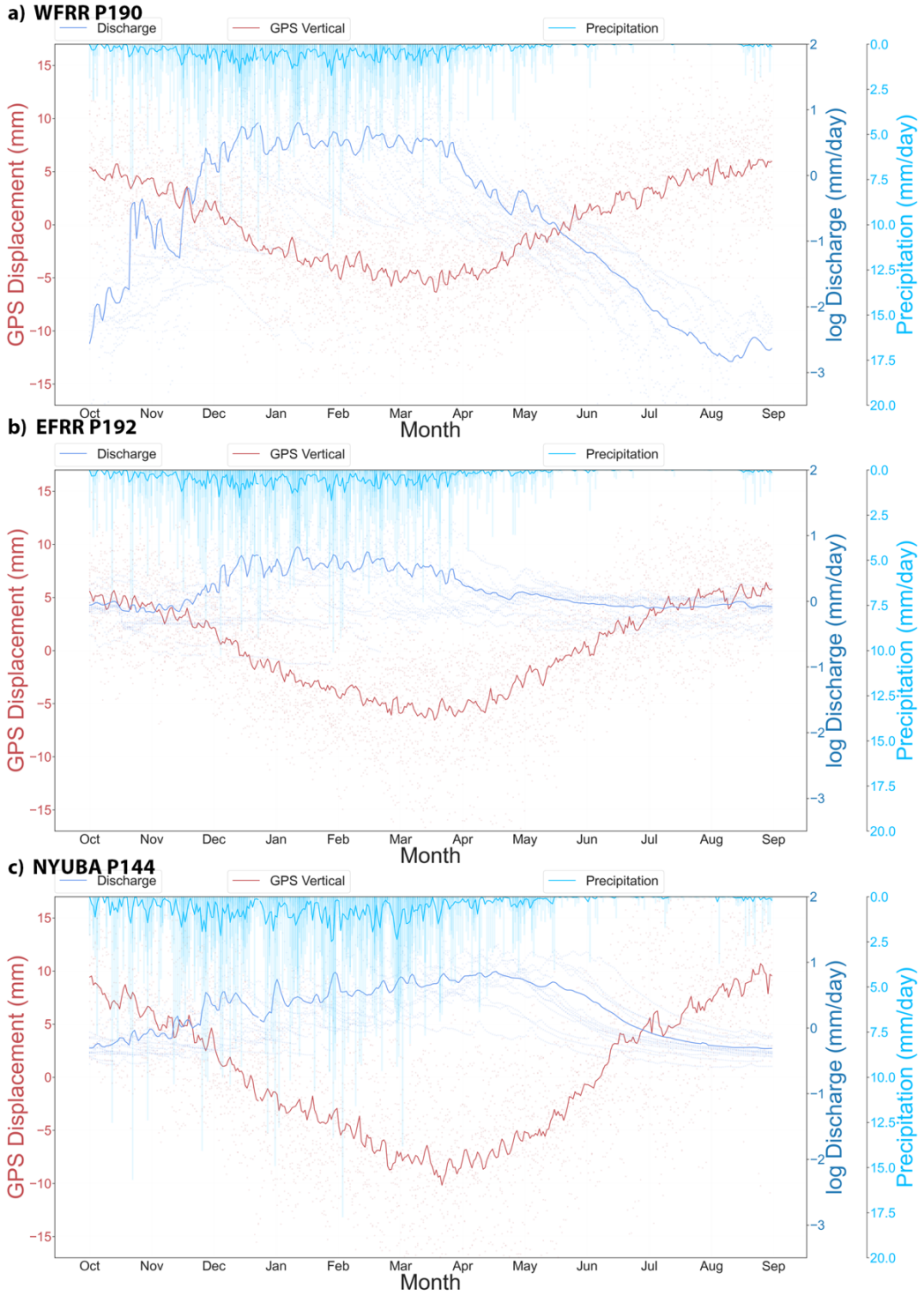

Figure 3.3: Time series for WFRR (a) and EFRR (b) and NYUBA (c) of average daily values (solid lines) for GPSVD in Camas Creek watershed. GPSVD is plotted (in red), log discharge (in dark blue), precipitation from GRIDMET (light blue), SWE (black), and temperature (reddish brown) from which SNOTEL). Daily values for individual years are plotted at reduced opacity. Horizontal axis displays the month of the water year beginning October 1st and ending on September 30th.

Qualitative analysis of average behavior in GPSVD-Q relationship:

Figure 4 displays the 30-day smoothed, daily - average behavior of the hydrologically isolated GPS vertical displacement to discharge relationship for each GPS site and stream gauge combination over the period of record. Values are color coded by month allowing us to follow the average behavior as the water year progresses and seasons change. These smoothed relationship plots form hysteresis loops where distinct seasonal loading patterns emerge between snow-dominated and rain-dominated/transitional watersheds.

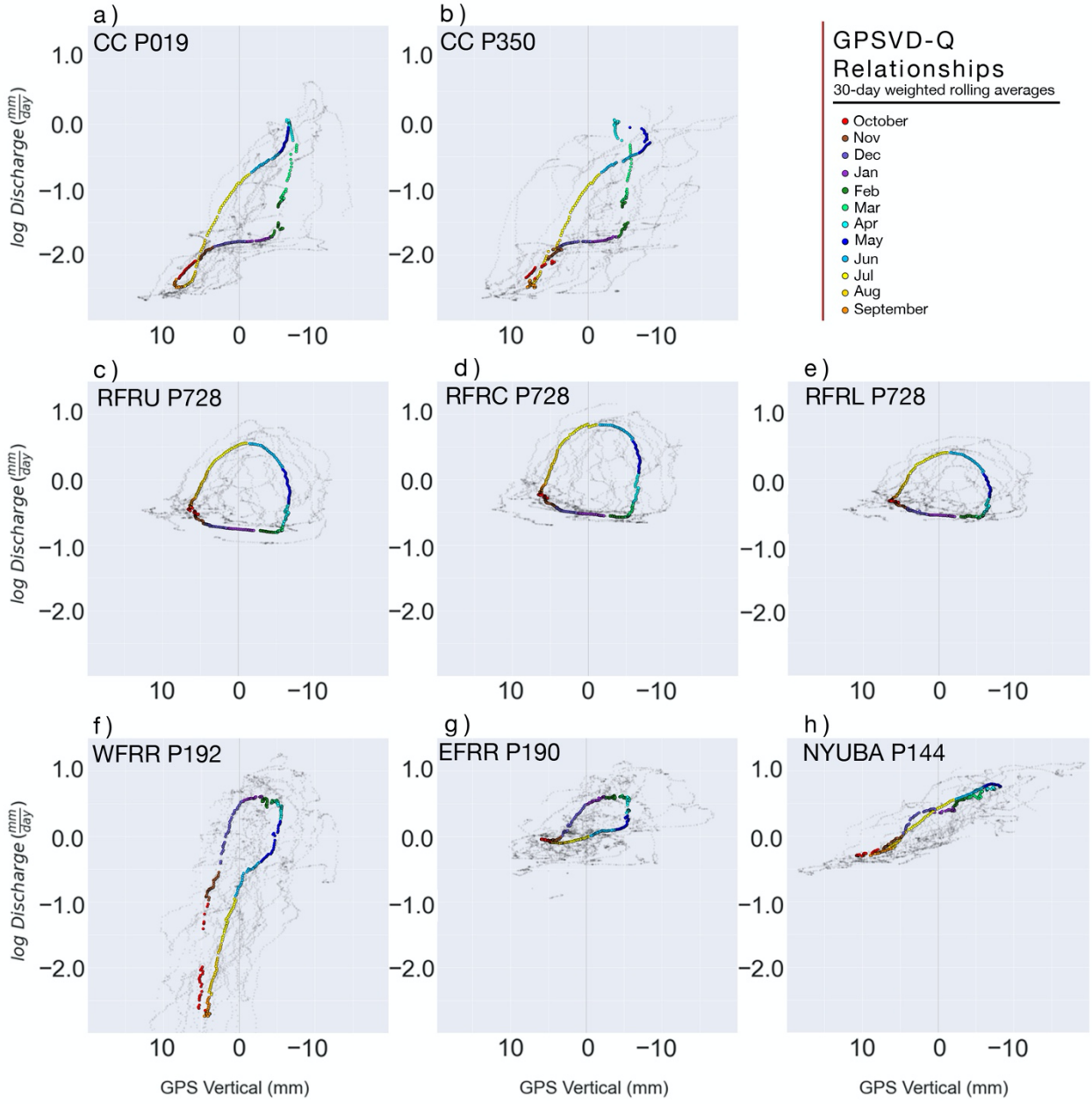

Figure 4: 30-day smoothed daily values for CC P019 (a), CC P350 (b), RFRU (c), RFRC (d), RFR (c), WFRR (f), EFRR (g), and NYUBA (h) where discharge(Q) is plotted against GPSVD as proxy for storage. Average behavior for daily values colored by month (circles). Smoothed daily values for individual water years are plotted at reduced opacity (grey circles). Positive GPS vertical represents upward displacement at the surface

(hydrologic unloading) and negative GPS displacement represents a downward surface response to hydrologic loading.

Temporal progression of the hysteresis loops in snow-dominated watersheds (Figure 4: a, b, c, d, and e) display GPSVD moving strongly in the negative direction without significant increases in discharge during winter months, with GPSVD total displacement between (~ 7.5-8 mm) at both Camas Creek sites and Roaring Fork watersheds. During winter terrestrial storage and stream connected storage diverge. This initiates a counterclockwise hysteresis progression when following the temporal progression, where in winter months, a nearly horizontal line is formed in the relationship plots when GPSVD is decreasing without significant changes in discharge. In spring months, terrestrial storage reconnects and discharge ascends sharply as it approaches peak discharge, and post-peak discharge GPSVD rebounds as discharge drops. This counterclockwise pattern is observed in both snow-dominated watersheds, CC and RFR. Duration of observed horizontal movement is relatively shorter in CC (~ 2 months, Dec. – Jan.) (Figure 4: a and b) compared to RFR (4+ months, Nov. – Feb.) (Figure 4: c, d, and e). RFR watersheds exhibit a slight decrease in discharge during this interval. Months associated with spring snowpack melting display a roughly vertical ascent in discharge while maintaining GPSVD until approaching or reaching peak discharge. CC's melt season lasts 3 months, on average, beginning in February and reaches peak discharge in April. RFR melts out for 3-4 months, March through mid-June. In RFR watersheds (Figure 4: c, d, and e), GPSVD starts out in vertical ascent but rebounds ~ 5-6 mm between the onset of melting and peak discharge. Major differences in hysteresis shape can be seen between CC and RFR watersheds as peak discharge is approached. RFR watershed GPSVD-discharge relationships (Figure 4: c, d, and e) transition slowly to hydrograph recession periods with a rounded transition. Conversely, CC (Figure 4: a and b), displays a sharp transition to hydrograph recession. CC experiences hydrograph recession ~ 4 months (May-Aug) and GPSVD rebounds ~15 mm, whereas RFR experiences hydrograph recession over ~3 months and rebounds ~8 mm from peak discharge to the end of the water year. GPSVD and discharge display an approximately linear relationship at the onset of hydrograph recession with decreasing discharge and increasing GPSVD in both snow-dominated watersheds.

Rain-dominated watersheds (Figure 4: f and g) show GPSVD and discharge ascending at the onset of the water year and move approximately linearly as the season progresses into winter where discharge plateaus briefly (< 1 month) at peak discharge. Post peak flows, discharge drops almost vertically for approximately 1 month without significant movement in GPSVD before transitioning to a hydrograph recession period where the GPSVD-discharge relationship behaves approximately linearly with discharge decreasing and GPSVD increasing. Relative to snow-dominated watersheds, hysteretic progression in rain-dominated watersheds move in an elongated (approximately linear) and seemingly clockwise temporal progression with 30-day smoothing. WFRR and EFRR (Figure 4: f and g) display similar watershed function behavior and average annual total GPSVD of 12.54 and 12.96 mm, respectively with precipitation accumulation occurring Oct-Mar. However, WFRR experiences ≈3 orders of magnitude greater difference in discharge, on average.

Finally, NYUBA (Figure 4h) displays strong linearity between GPSVD and discharge throughout the water year. We observe ~20 mm of average annual total GPSVD with precipitation accumulation occurring ~8 months (Oct.-May) and hydrograph recession coinciding with GPSVD rebound over 4 months (Jun.-Sep.). During hydrograph recession

months, less scatter is observed indicating this interval has a stronger GPSVD-discharge relationship relative to the rest of the water year.

Isolating Hydrograph Recession GPSVD-discharge Relationships

When isolating our analysis to periods of seasonal hydrograph recession, all watersheds display strong GPSVD-discharge relationships (Figures 5.1 – 5.3) from mid-hydrograph recession to baseflow, for both daily values (blue diamonds) and average behavior POR values (red dots). In these plots, we observe a curvilinear relationship curve similar to those expected in storage-discharge relationship plots (Kirchner, 2009). RFR watersheds (Figure 5.2: a, b, and c) are the exception and display strong linearity through this recession analysis period.

Mountainous mid-elevation GPS sites, CC P019 (Figure 5.1 a) and NYUBA (Figure 5.3 c), display the least amount of scatter relative to other sites on an interannual basis (blue diamonds), as displayed by dense clustering of GPSVD-discharge relationships during hydrograph recession periods, especially when transitioning from mid-hydrograph recession to baseflows. Snow-dominant, high elevation GPS station locations display greater variability in interannual GPSVD-discharge relationships (Figure 5.1 b, Figure 5.2: a, b, and c).

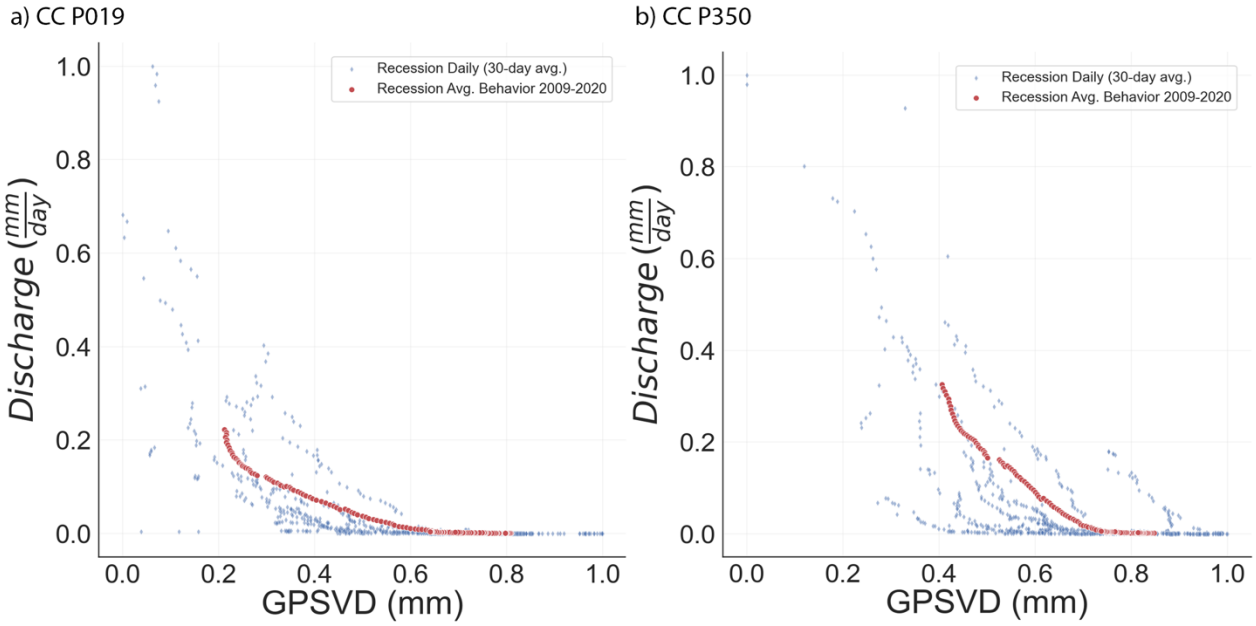

Figure 5.1: GPSVD-discharge relationship in CC during hydrograph recession periods meeting criteria of (P,ET << Q) plotted (in blue) and period of record average behavior during recession periods (in red).

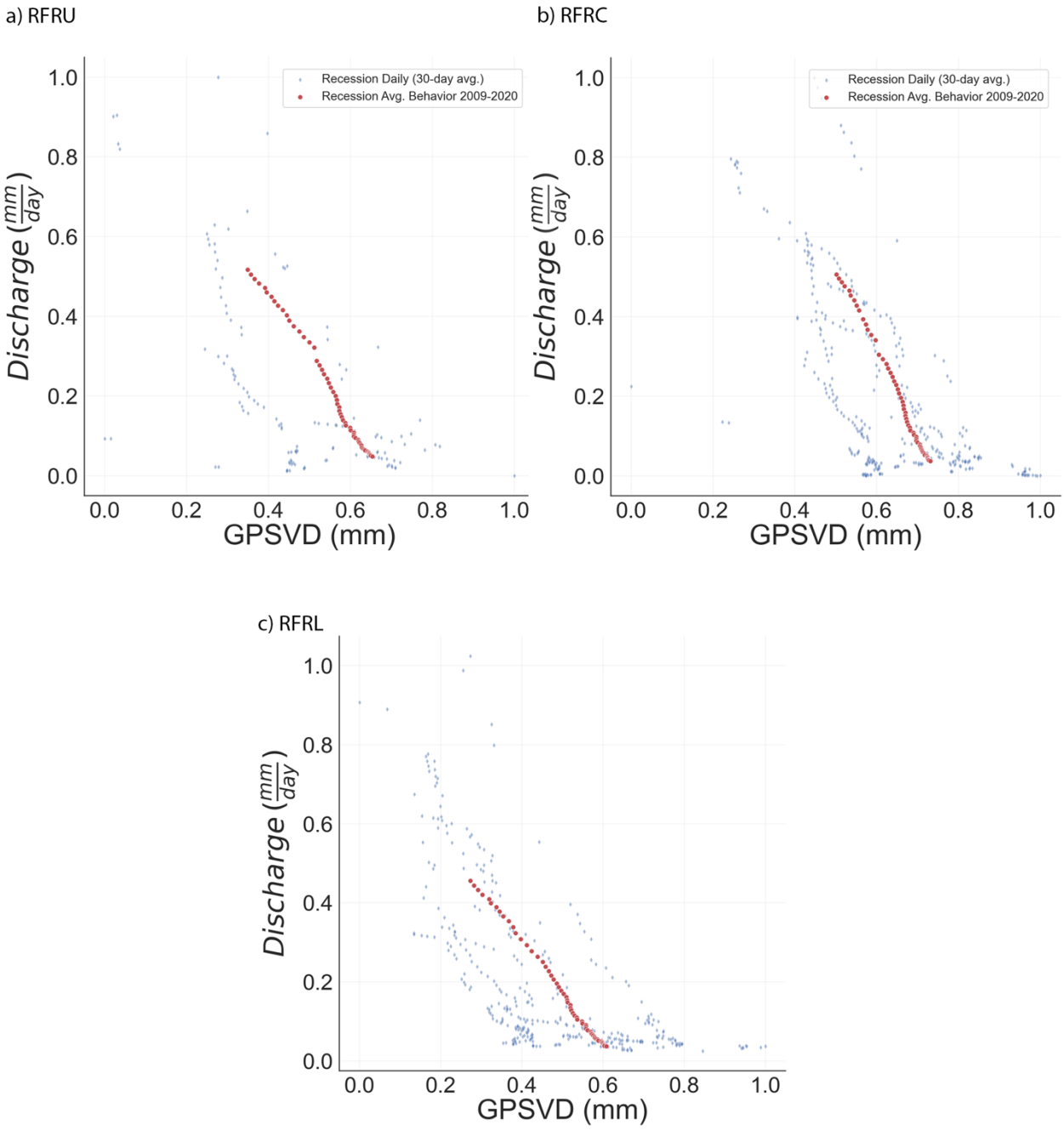

Figure 5.2: GPSVD-discharge relationship in RFR during hydrograph recession periods meeting criteria of (P,ET << Q) plotted (in blue) and period of record average behavior during recession periods (in red).

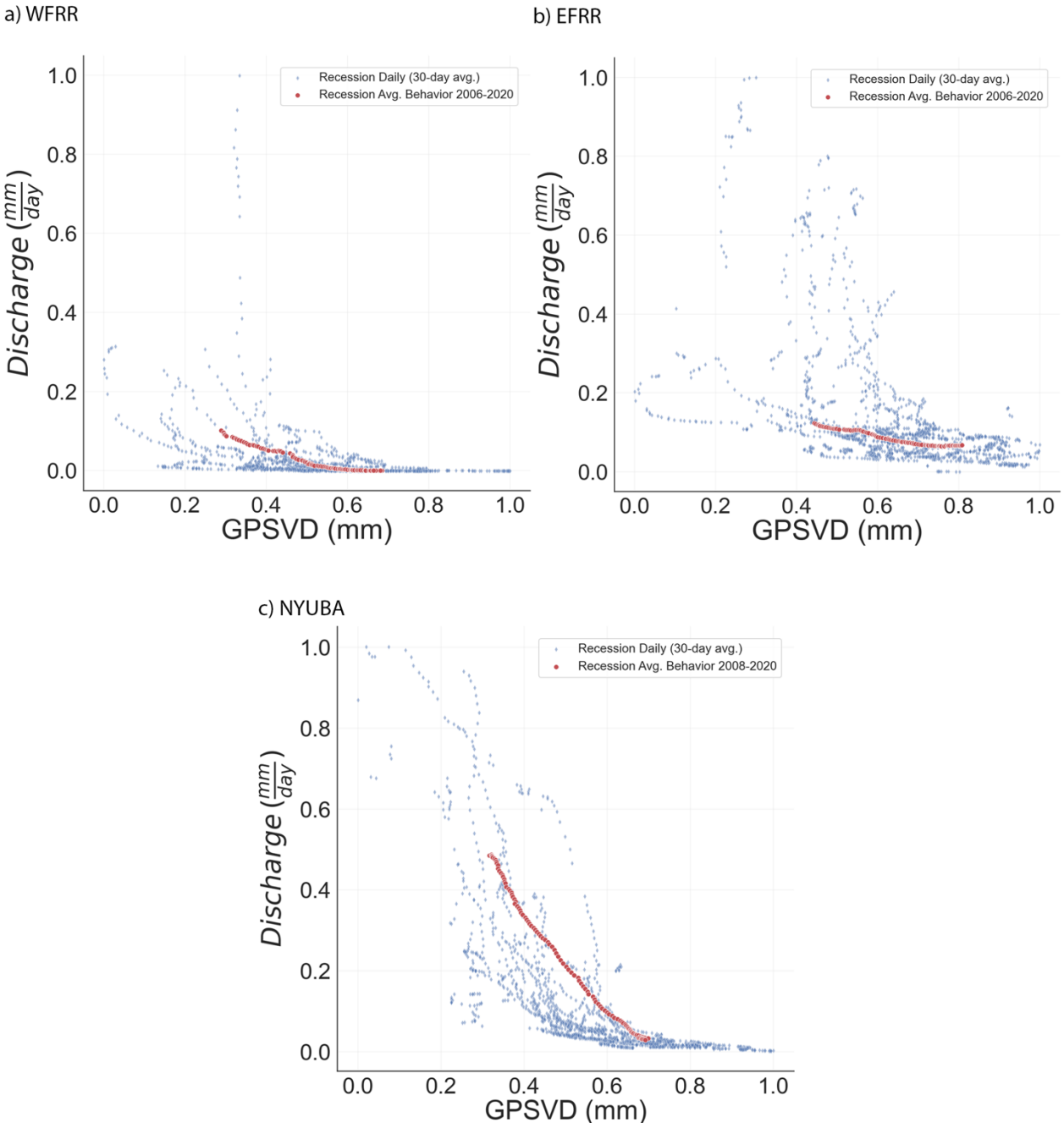

Figure 5.3: GPSVD-discharge relationship in transitional (c) and rain dominated watersheds (a, b) during hydrograph recession periods meeting criteria of (P,ET << Q) plotted (in blue) and period of record average behavior during recession periods (in red).

The curvature of GPSVD-discharge interannual relationships appear to change as horizontal shifts in GPSVD occur. This is displayed most prominently at CC's high elevation GPS site, CC P350 (Figure 5.1 b), by interannual relationship plots (blue) on both sides of the average behavior curve (red) where the end members (blue) display different relationships. As GPSVD moves higher than average the relationship becomes more linear. And when GPSVD moves lower than average the relationship becomes increasingly curvilinear. Similar observations are made in WFRR, EFRR, and NYUBA (Figure 5.3 a, b, and c) and CC P019 (Figure 5.1 a). RFR watersheds (Figure 5.2) maintain a linear GPSVD-discharge relationship but also display shifts leftward and rightward on the horizontal GPSVD axis.

Watershed Sensitivity Analysis

Linear regression analysis of discharge rate versus increments of discharge during recession periods provide parameterization of the power law function (Equation 4) and the central tendency of transport processes rates unique to each watershed (Kirchner, 2009). The exponent of the power law function has the greatest influence and describes the rate at which stream connected storage is released from a watershed when conditions meet (P, ET << Q). Watersheds typically display ranges of exponent values between 1 and 2 (Kirchner, 2009). Exponent values closer to 2 indicate flashier watershed systems and lower exponents indicate watersheds displaying relatively longer residence times.

Our analysis (Figures 6.1 – 6.3) found exponent values ranging from (β = 0.92 to 1.54) with WFRR (Figure 6.3 a) exhibiting the lowest β value indicating less sensitivity and NYUBA (Figure 6.3 c) indicating the flashiest watershed of in this study (β = 1.54). Snow-dominated watersheds display β ranging from (0.98 to 1.34). In rain-dominated, small-scale watersheds WFRR (238 km^2) and EFRR (259 km^2), we found β values of 0.92 and 1.17, respectively.

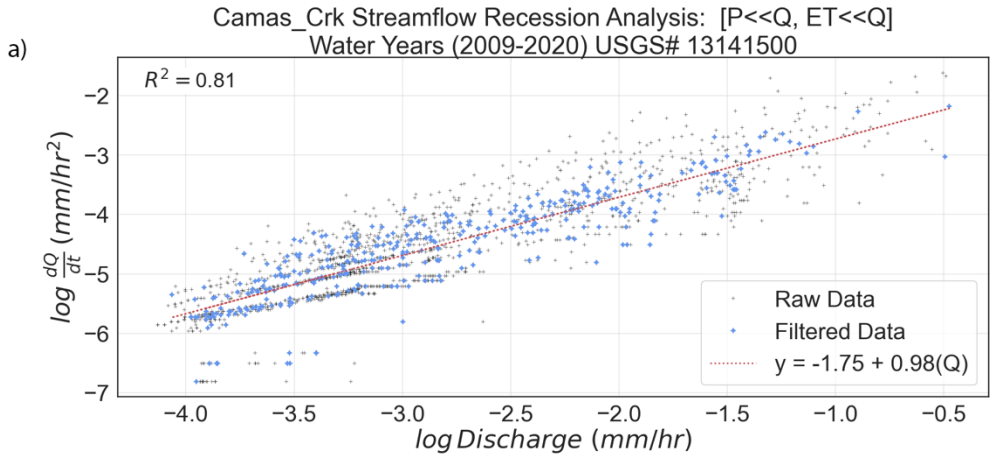

Figure 6.1: Log-log linear regression plots used for power law parameterization for raw daily discharge rate following Kirchner (2009) in CC. (Black points) are all values where streamflow recession occurs over the period of study and (blue points) represent filtered data points matching criteria of Kirchner (2009) method (P, ET << Q) used for parameterization. (Red dotted line) is line of best fit and R^2 values (upper left) provide a metric for goodness of fit.

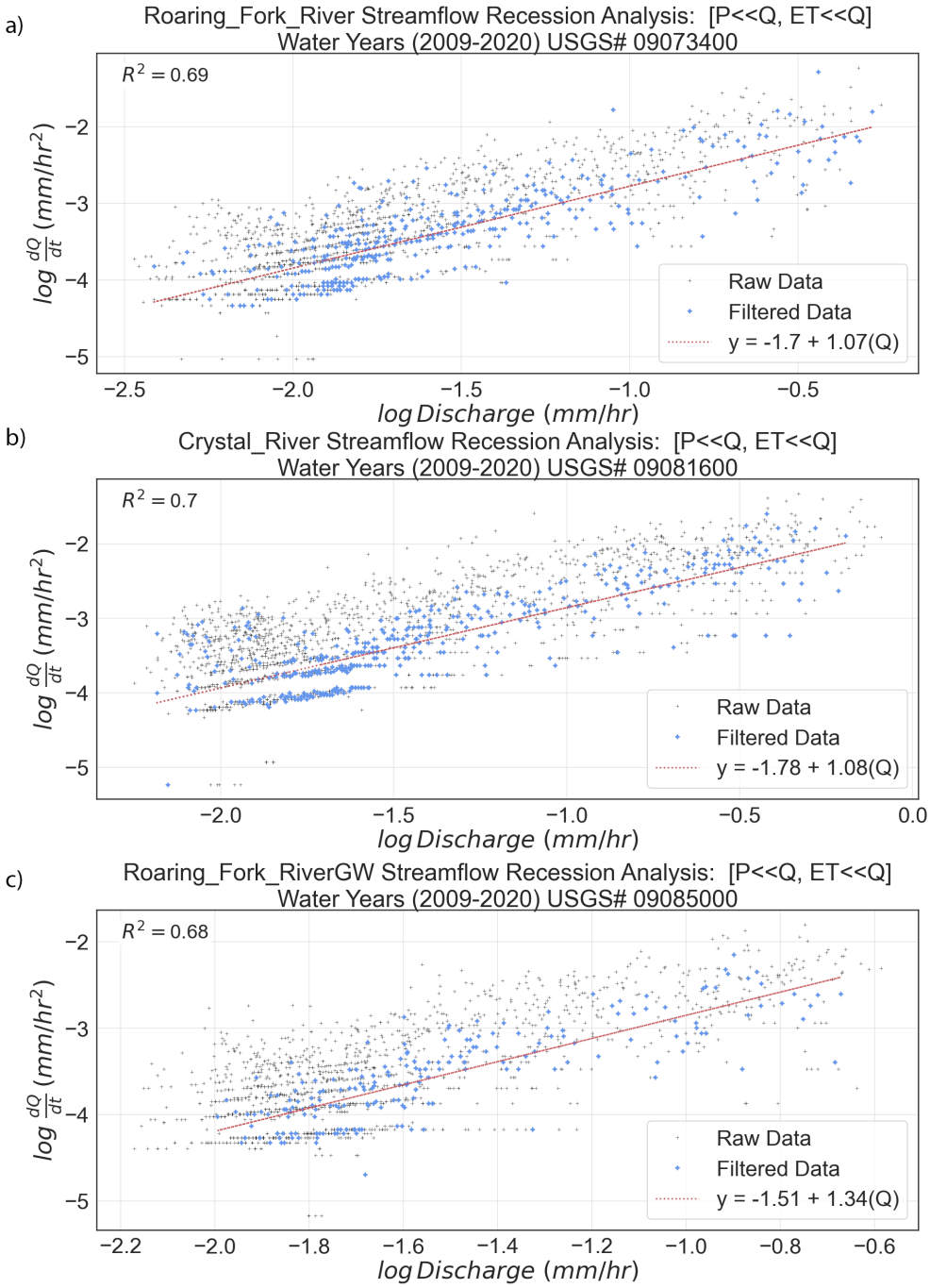

Figure 6.2: Log-log linear regression plots used for power law parameterization for raw daily discharge rate following Kirchner (2009) in RFRU (a), RFRC (b), and RFRL (c). (Black points) are all values where streamflow recession occurs over the period of study and (blue points) represent filtered data points matching criteria of Kirchner (2009) method (P, ET << Q) used for parameterization. (Red dotted line) is line of best fit and R^2values (upper left) provide a metric for goodness of fit.

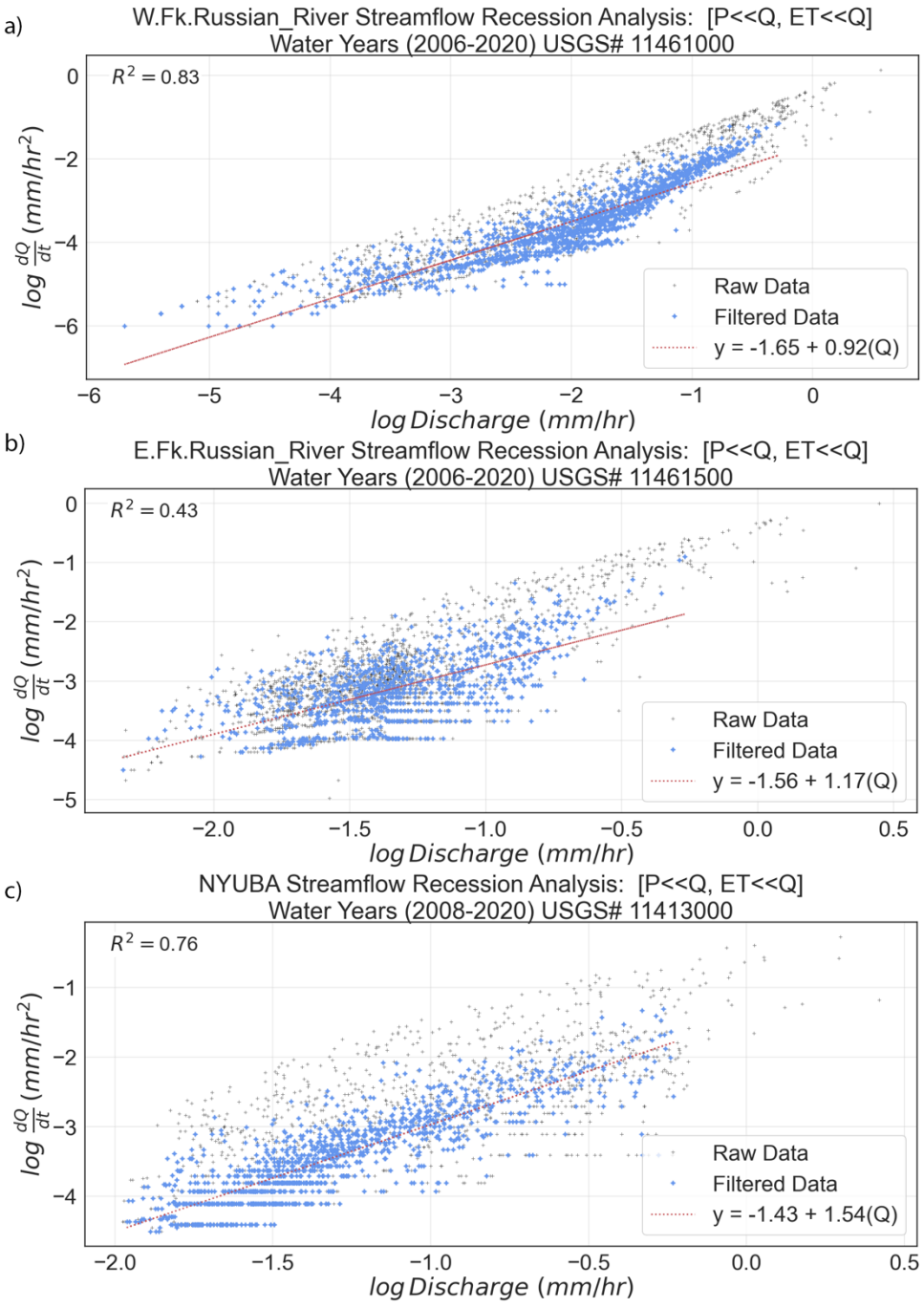

Figure 6.3: Log-log linear regression plots used for power law parameterization for raw daily discharge rate following Kirchner (2009) in WFRR (a), EFRR (b), and NYUBA (c). (Black points) are all values where streamflow recession occurs over the period of study and (blue points) represent filtered data points matching criteria of Kirchner (2009) method (P, ET << Q) used for parameterization. (Red dotted line) is line of best fit and R^2values (upper left) provide a metric for goodness of fit.

Hydrograph Recession GPSVD-DIS Relationships

Using our parameterization of discharge sensitivity (Equations 4 and 6) we calculate discharge inferred storage (DIS) following Kirchner (2009). We plot the relationship between DIS and GPSVD and isolate our analysis to periods of seasonal hydrograph recession. All watersheds display strong GPSVD-DIS relationships (Figures 7.1 – 7.3) from mid-hydrograph recession to baseflow, for both daily values (blue diamonds) and average behavior POR values (red dots). As DIS is directly inferred from discharge, the relationship plots between GPSVD-discharge and GPSVD-DIS are nearly identical with the difference in R^2 being < 0.2.

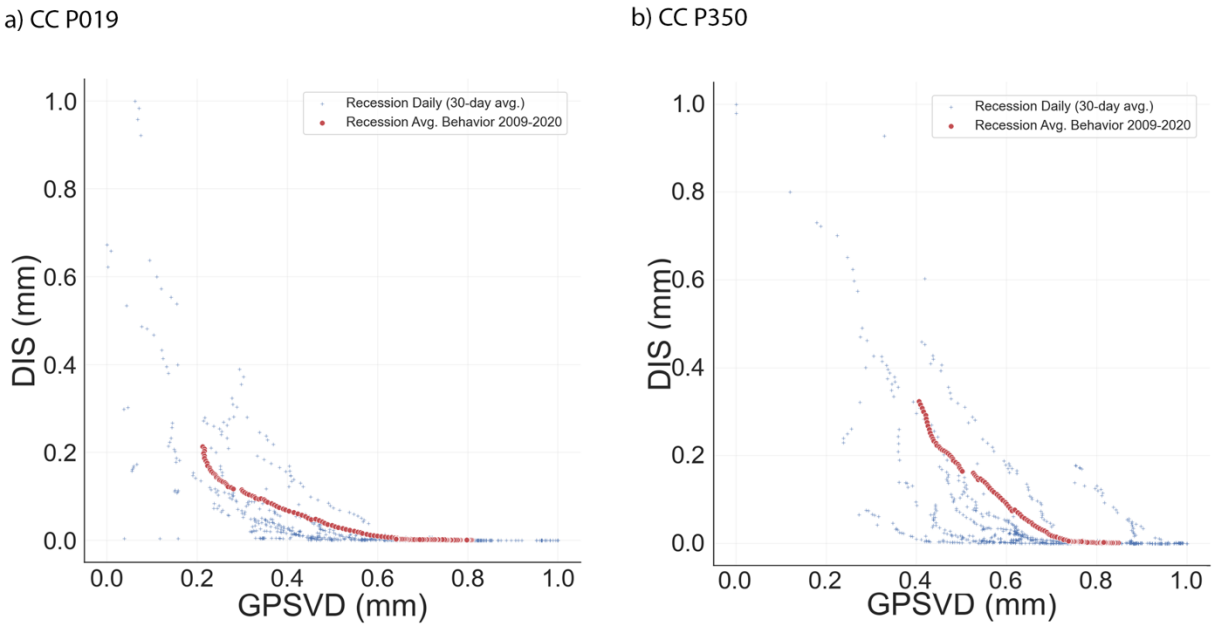

Figure 7.1: GPSVD-discharge relationship for CC P019 (a) and CC P350 (b) during hydrograph recession periods meeting criteria of (P,ET << Q) plotted (in blue) and period of record average behavior during recession periods (in red).

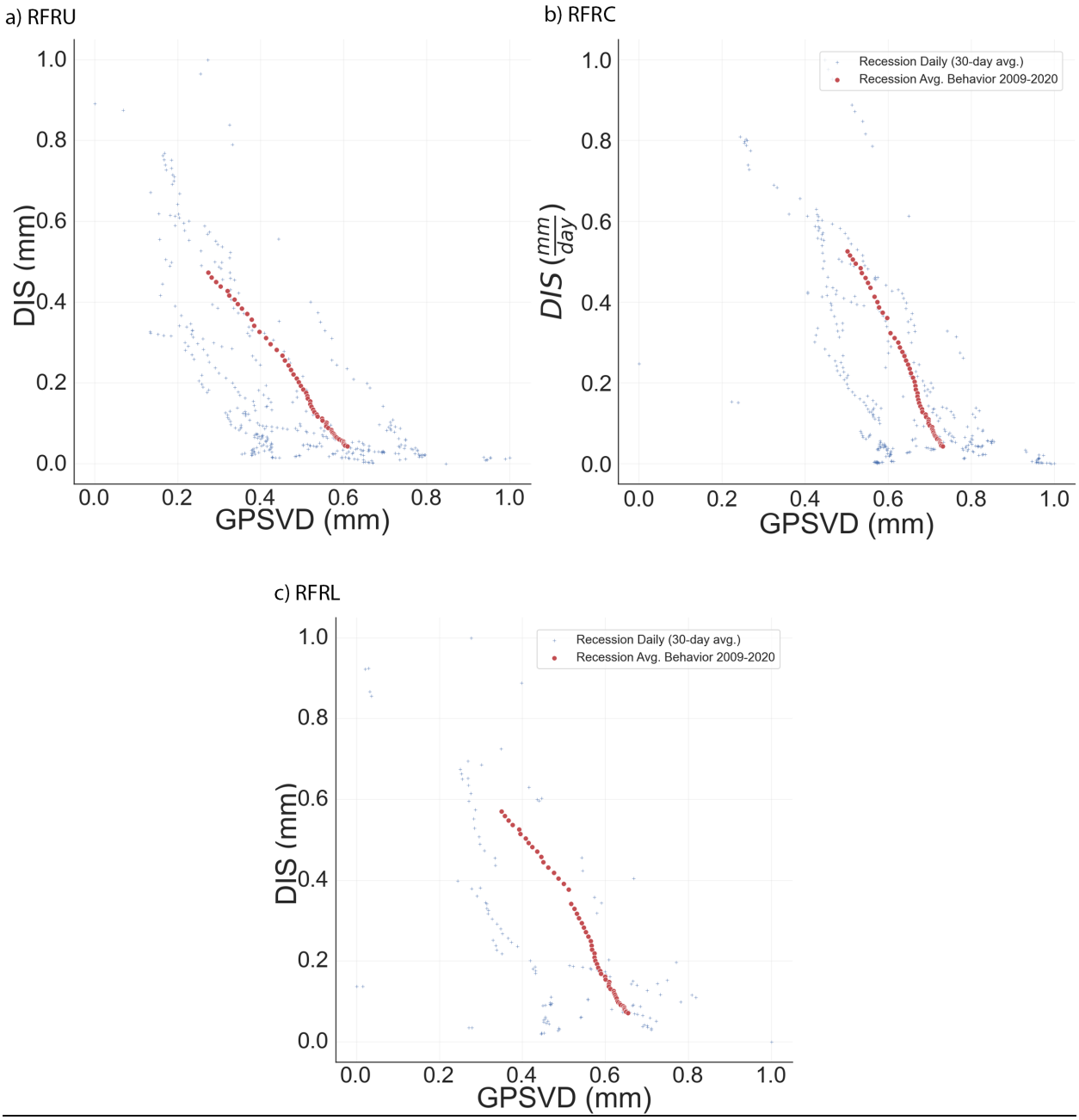

Figure 7.2: GPSVD-discharge relationship RFRU (a) RFRC (b) and RFRL (c) during hydrograph recession periods meeting criteria of (P,ET << Q) plotted (in blue) and period of record average behavior during recession periods (in red).

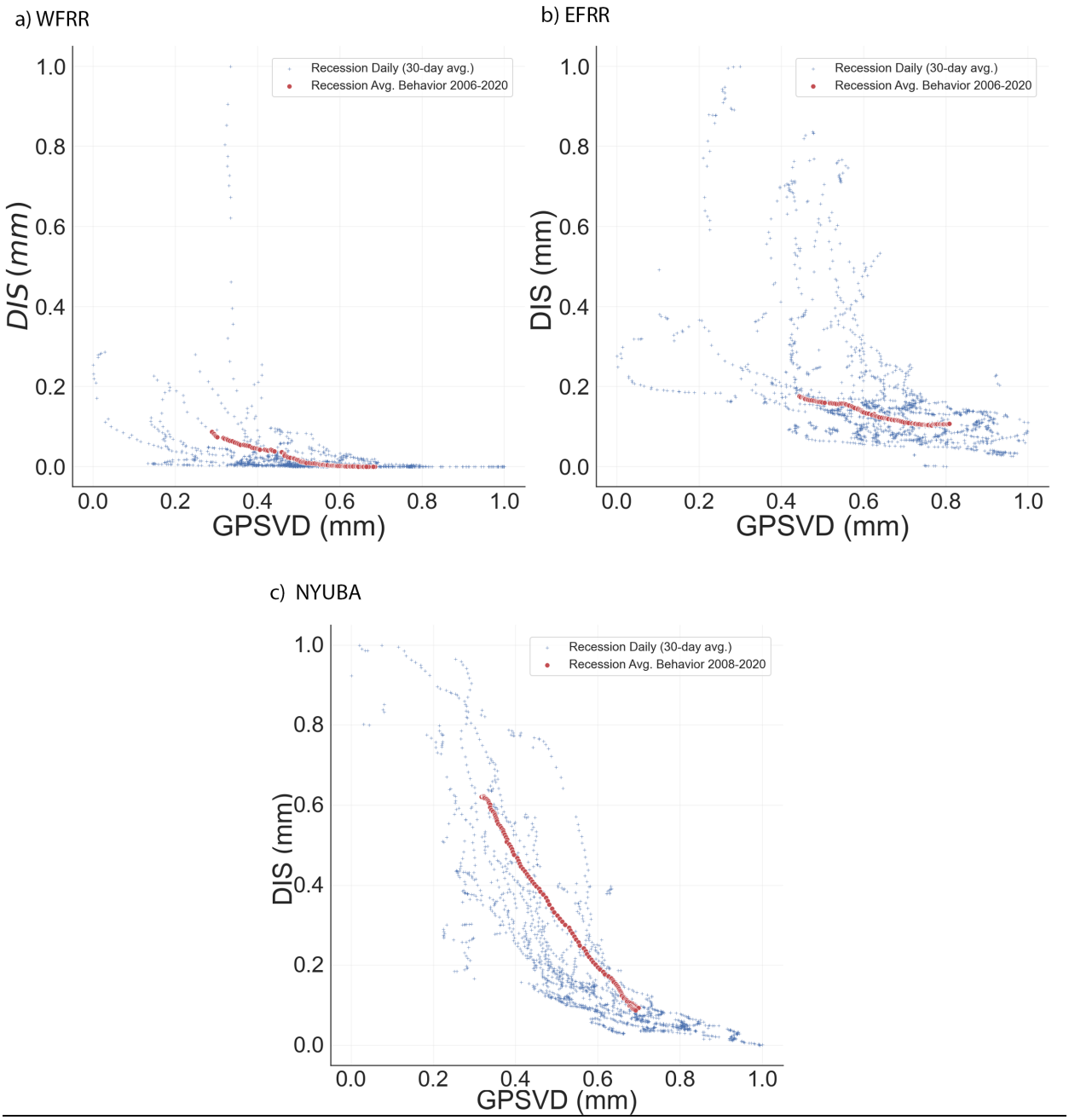

Figure 7.3: GPSVD-discharge relationship WFRR (a) EFRR (b) and NYUBA (c) during hydrograph recession periods meeting criteria of (P,ET << Q) plotted (in blue) and period of record average behavior during recession periods (in red).

Statistical Analysis:

Figure 8.1 visually summarizes our R^2 analysis for GPSVD-discharge relationships and GPSVD-DIS relationships (Figure 8.2) in each of the watersheds in this study. As DIS is inferred from discharge, the figures are almost identical and R^2 values (Table 1) are practically identical (R^2 +/- 0.2). The bar charts display R^2 analysis results with 1, 3, 14, and 30-day rolling weighted daily averages for all smoothed values, average period of record daily values (POR), and for periods where we isolated the data to strictly hydrograph recession periods meeting the criteria according to Kirchner (2009) for parameterizing discharge rates and watershed characterization.

At most study site locations, the GPSVD-discharge daily values display improvement in R^2 values with increased smoothing. Weak relationships for all watershed ($R^2 < 0.1$) were found using all daily smoothed data except in NYUBA, CC P350, and CC P019, where 30-day smoothing provides R^2 values of 0.45 (+0.24), 0.34 (+0.13), and 0.23 (+0.19), respectively (Figure 8.1 or Table 1). Analyzing daily smoothed values and isolating our analysis to hydrograph recession periods, we observe slight gains in R^2 values, but the GPSVD-discharge relationships maintain weak agreement ($R^2 < 0.38$). GPSVD-DIS relationships using unsmoothed daily values are identical in all study watersheds except for NYUBA which displays a (+ 0.13) gain in R^2 compared to GPSVD-discharge. GPSVD-discharge relationships display improvement (+0.12 to +0.28) in R^2 values in NYUBA ($R^2 = 0.62$), CC P019 ($R^2 = 0.34$), and CC P350 ($R^2 = 0.34$) with 30-day smoothing. GPSVD-DIS relationships are again, nearly identical with differences in $R^2 < 0.2$ except in NYUBA showing strengthening in R^2 (+ 0.11).

Average daily behavior of the GPSVD-discharge relationship over the period of record (POR) provides improvement in all but the RFR watersheds ($R^2 < 0.15$) and again, the relationship strengthens with increased smoothing providing R^2 values ranging from (0.32 to 0.92) with 30-day smoothing. POR GPSVD-discharge relationships significantly strengthen at all sites when isolating analysis to hydrograph recession periods with R^2 values ranging from (0.20 to 0.91) with 3-day smoothing and (0.78 to 0.96) with 30-day smoothing and GPSVD-DIS R^2 values ranging (0.78 to 0.98) (Table 1).

Overall, we find stronger relationships with increased smoothing when isolating our analysis to recession periods, and the strongest relationships are found using the average daily behavior of variables, POR, and isolating our analysis to seasonal hydrograph recession periods. We note that in CC P019 POR recession R^2 values are better when using 7-day weighted averages vs. 14 or 30-day smoothing. The same happens in EFRR P190 except the 14-day weighted average outperforms those obtained with 30-day smoothing.

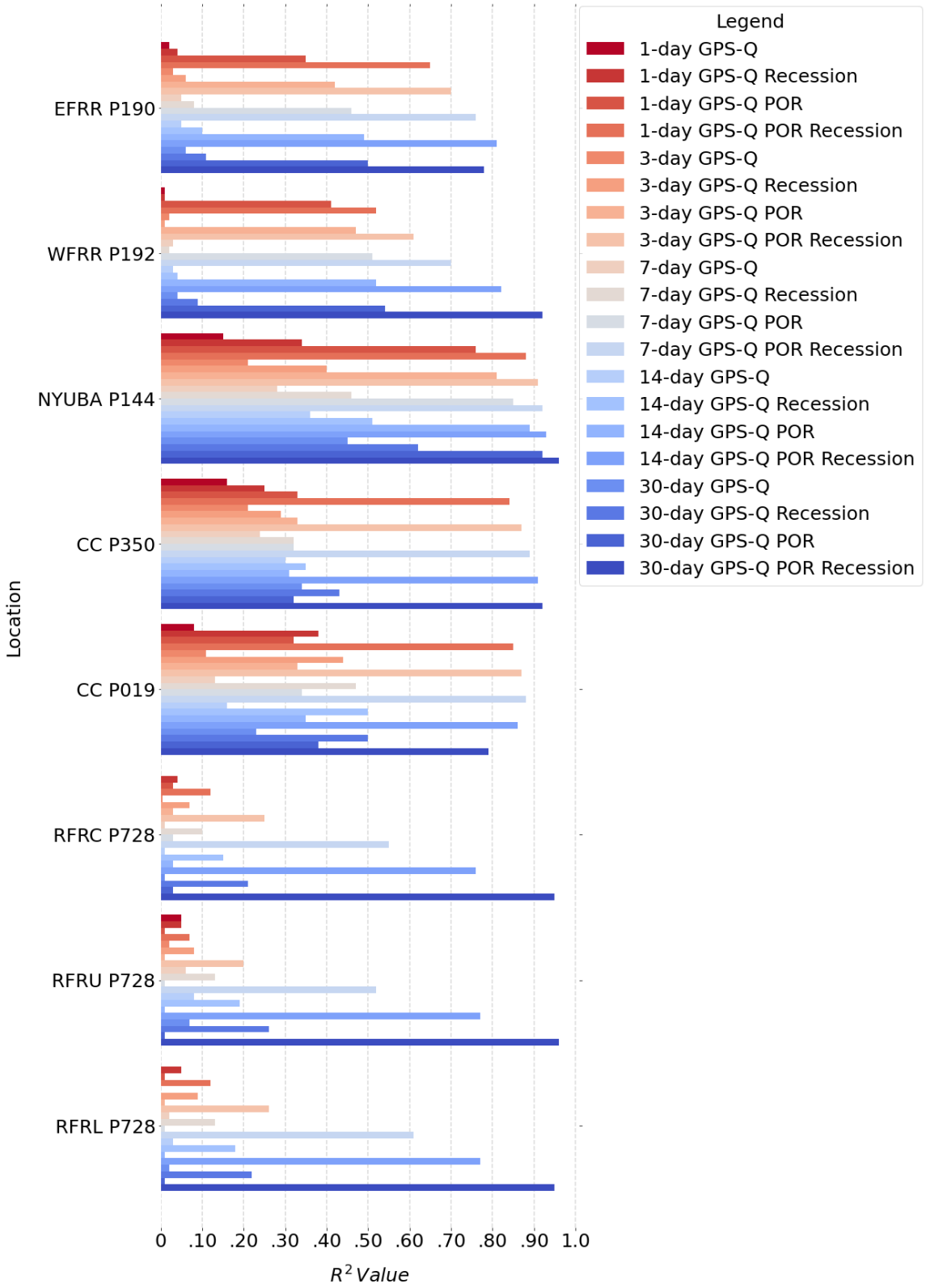

***Figure 8.1**: R^2 metrics for GPSVD-discharge relationship for (1, 3, 7, 14, and 30-day) rolling weighted average daily values for full time series, during periods of recession only (Recession), average values over the period of record (POR), and average behavior over the period of record during recession periods only (POR Recession).*

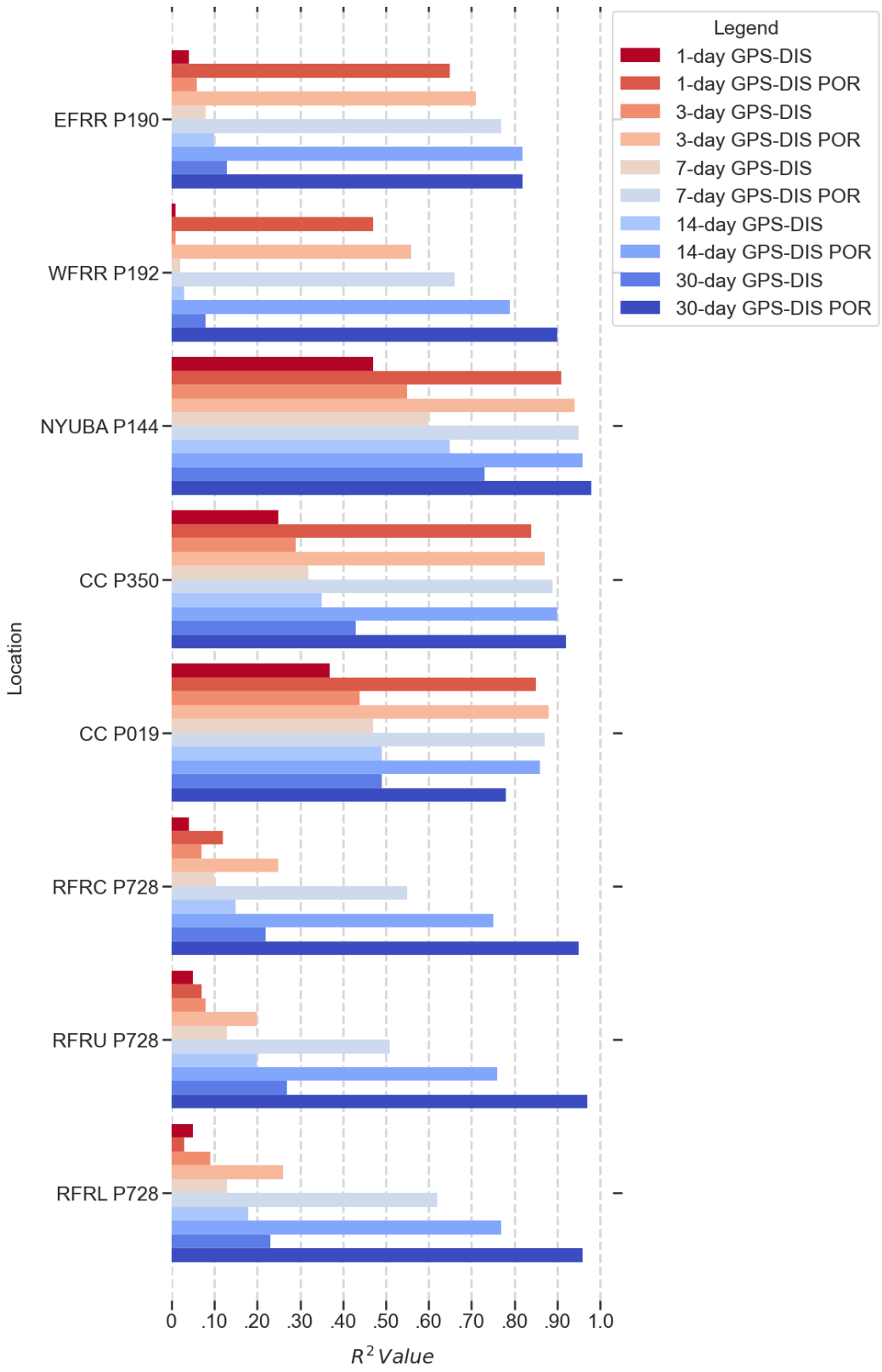

***Figure 8.2**: R^2 metrics for GPSVD-DIS relationship for (1, 3, 7, 14, and 30-day) rolling weighted average daily values for GPS-DIS relationships isolated to periods of hydrograph recession, average recession values over the period of record (POR).*

***Table 1**: R^2 metrics for GPSVD-discharge relationship & GPSVD-DIS for (3, 14, and 30-day) rolling weighted average values for full time series and during hydrograph recession. Raw daily values (RAW) under yellow header and average values over period of record (POR) under orange headers.*

1-day avg.	RAW	recession	recession	POR	recession	recession
Site	**GPSVD-Q**	**GPSVD-Q**	**GPSVD-DIS**	**GPSVD-Q**	**GPSVD-Q**	**GPSVD-DIS**
EFRR	0.02	0.04	0.04	0.35	0.65	0.65
WFRR	0.01	0.01	0.01	0.41	0.52	0.47
NYUBA	0.15	0.34	0.47	0.76	0.88	0.91
CC P350	0.16	0.25	0.25	0.33	0.84	0.84
CC P019	0.08	0.38	0.37	0.32	0.85	0.85
RFRC	0.00	0.04	0.04	0.03	0.12	0.12
RFRU	0.05	0.05	0.05	0.01	0.07	0.07
RFRL	0.0002	0.05	0.05	0.01	0.12	0.03
3-day avg.	RAW	recession	recession	POR	recession	recession
Site	**GPSVD-Q**	**GPSVD-Q**	**GPSVD-DIS**	**GPSVD-Q**	**GPSVD-Q**	**GPSVD-DIS**
EFRR	0.03	0.06	0.06	0.42	0.7	0.71
WFRR	0.02	0.01	0.01	0.47	0.61	0.56
NYUBA	0.21	0.4	0.55	0.81	0.91	0.94
CC P350	0.21	0.29	0.29	0.33	0.87	0.87
CC P019	0.11	0.44	0.44	0.33	0.87	0.88
RFRC	0.004	0.07	0.07	0.03	0.25	0.25
RFRU	0.02	0.08	0.08	0.01	0.2	0.2
RFRL	0.00	0.09	0.09	0.01	0.26	0.26
7-day avg.	RAW	recession	recession	POR	recession	recession
Site	**GPSVD-Q**	**GPSVD-Q**	**GPSVD-DIS**	**GPSVD-Q**	**GPSVD-Q**	**GPSVD-DIS**
EFRR	0.05	0.08	0.08	0.46	0.76	0.77
WFRR	0.03	0.02	0.02	0.51	0.7	0.66
NYUBA	0.28	0.46	0.6	0.85	0.92	0.95
CC P350	0.24	0.32	0.32	0.32	0.89	0.89
CC P019	0.13	0.47	0.47	0.34	0.88	0.87
RFRC	0.01	0.1	0.1	0.03	0.55	0.55
RFRU	0.06	0.13	0.13	0.01	0.52	0.51
RFRL	0.02	0.13	0.13	0.01	0.61	0.62
14-day avg.	RAW	recession	recession	POR	recession	recession
Site	**GPSVD-Q**	**GPSVD-Q**	**GPSVD-DIS**	**GPSVD-Q**	**GPSVD-Q**	**GPSVD-DIS**
EFRR	0.05	0.1	0.1	0.49	0.81	0.82
WFRR	0.03	0.04	0.03	0.52	0.82	0.79
NYUBA	0.36	0.51	0.65	0.89	0.93	0.96
CC P350	0.3	0.35	0.35	0.31	0.91	0.9
CC P019	0.16	0.5	0.49	0.35	0.86	0.86
RFRC	0.01	0.15	0.15	0.03	0.76	0.75
RFRU	0.08	0.19	0.2	0.01	0.77	0.76
RFRL	0.03	0.18	0.18	0.01	0.77	0.77
30-day avg.	RAW	recession	recession	POR	recession	recession
Site	**GPSVD-Q**	**GPSVD-Q**	**GPSVD-DIS**	**GPSVD-Q**	**GPSVD-Q**	**GPSVD-DIS**
EFRR	0.06	0.11	0.13	0.5	0.78	0.82
WFRR	0.04	0.09	0.08	0.54	0.92	0.9
NYUBA	0.45	0.62	0.73	0.92	0.96	0.98
CC P350	0.34	0.43	0.43	0.32	0.92	0.92
CC P019	0.23	0.5	0.49	0.38	0.79	0.78
RFRC	0.01	0.21	0.22	0.03	0.95	0.95
RFRU	0.07	0.26	0.27	0.01	0.96	0.97
RFRL	0.02	0.22	0.23	0.01	0.95	0.96

RGPSS-GPSVD and discharge comparisons:

Timeseries plots (Figures 9.1 – 9.3) assist qualitative comparison of RGPSS to DIS storage estimates from October 2008 through September 2020. We observe that RGPSS roughly aligns with seasonal patterns of storage gains and losses with DIS in all watersheds. Broadly, RGPSS appears to respond in sync with DIS storage estimates but exhibits greater variability, exhibiting large gains and losses in storage that are not captured in DIS estimates. For example, in RFRC (Figure 9.2 b), water years 2011 through 2019 show near perfect alignment with DIS during hydrograph recession but fall well below what DIS storage can capture. And in NYUBA (Figure 9.3 c), years with higher DIS estimates correspond to RGPSS higher estimates, and lower discharge years (water years 2014 and 2015) correspond to RGPSS estimates that trend below the average RGPSS estimate. RGPSS displays a downward trend in storage estimations over the period in all RFR watersheds (Figure 9.2) and an upward trend in CC watersheds (Figure 9.1). Overall, similar cyclical patterns are observed in every watershed studied but RGPSS displays greater variability when predicting storage relative to DIS.

Next, we compare RGPSS and GPSVD relationships to discharge to see how GPSVD, as a proxy for storage, compares to regional storage inferences from RGPSS (Table 2). Limiting the comparison to hydrograph recession periods, RGPSS-Q and GPSVD-Q relationships are in close agreement (R^2 < +/- 0.13) in EFRR, WFRR, NYUBA, and CC P350 but display weak to moderate relationships to discharge. However, GPSVD-Q displays improved relationships relative to RGPSS-Q in CC P019, RFRC, RFRU, and RFRL, when limiting analysis to recession periods, displaying moderate relationships with R^2 values increasing +0.39, +0.20, +0.31, and +0.18, respectively.

Next, we analyze agreement between two independent inferences of storage, RGPSS and DIS (Table 2). Our results indicate weak to moderate agreement in NYUBA, RFRC, and RFRL with R^2 values ranging from (0.31 to 0.56). All other watersheds show weak agreement between both inferred storage estimates (R^2 < 0.3).

GPSVD-DIS relationships offer insight as to how well GPSVD can be used as a proxy for storage. GPSVD-DIS relationships isolated to recession periods with 30-day smoothing display R^2 values ranging from (0.17 to 0.63) exhibiting weak to moderate agreement in NYUBA, both CC sites, and all RFR watersheds (Table 2). Compared to RGPSS-DIS relationships, most GPSVD-DIS relationships show increased R^2 values (+0.04 to +0.37) during hydrograph recession periods except for EFRR (-0.09).

Finally, we compare GPSVD-RGPSS to GPSVD-DIS (Table 2) to compare relationships between both independent inferences of storage and local downward displacement in GPSVD. RGPSS exhibits a stronger relationship to GPSVD in EFRR relative to GPSVD-DIS relationships with R^2 difference of (+0.43) and exhibits a moderately strong relationship (R^2 = 0.60). Minimal gains in R^2 (<0.1) were observed in WFRR, NYUBA, and CC P350 showing relative agreement between GPSVD-RGPSS and GPSVD-DIS relationships in these watersheds. However, GPSVD-DIS R^2 values show better agreement in CC P019 (+0.46), RFRC (+0.43), RFRU (+0.40), and RFRL (+0.45) and exhibit moderate agreement between GPSVD-DIS relationships with a large improvement compared to RGPSS in these watersheds.

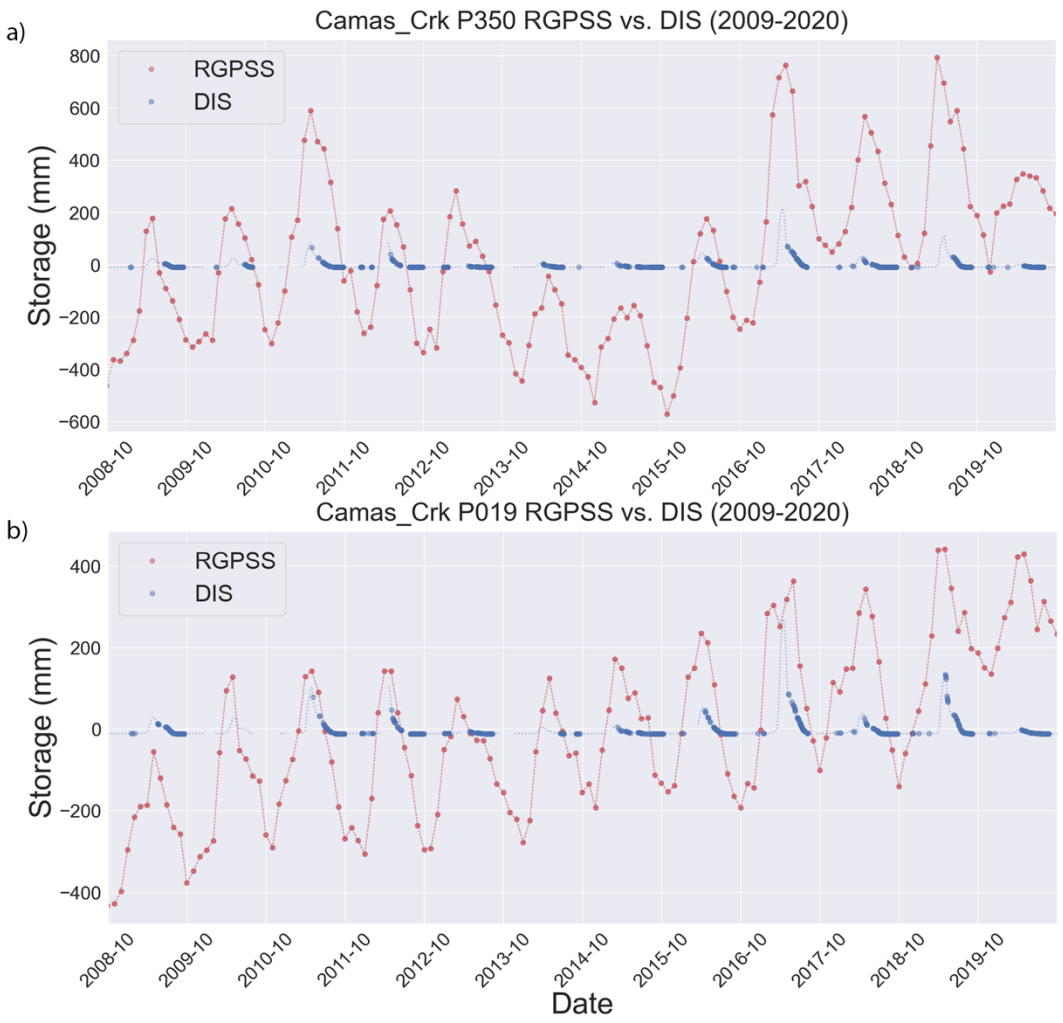

Figure 9.1*: CC RGPSS vs. DIS time series comparison of monthly RGPSS (red dots) and 30-day monthly average DIS (blue dots). DIS via Kirchner method is valid only during periods of recession meeting (P,ET <<Q) but blue dotted lines predict DIS for remainder of year and do not include P or ET and are included for reference and for following temporal progression of storage estimates.*

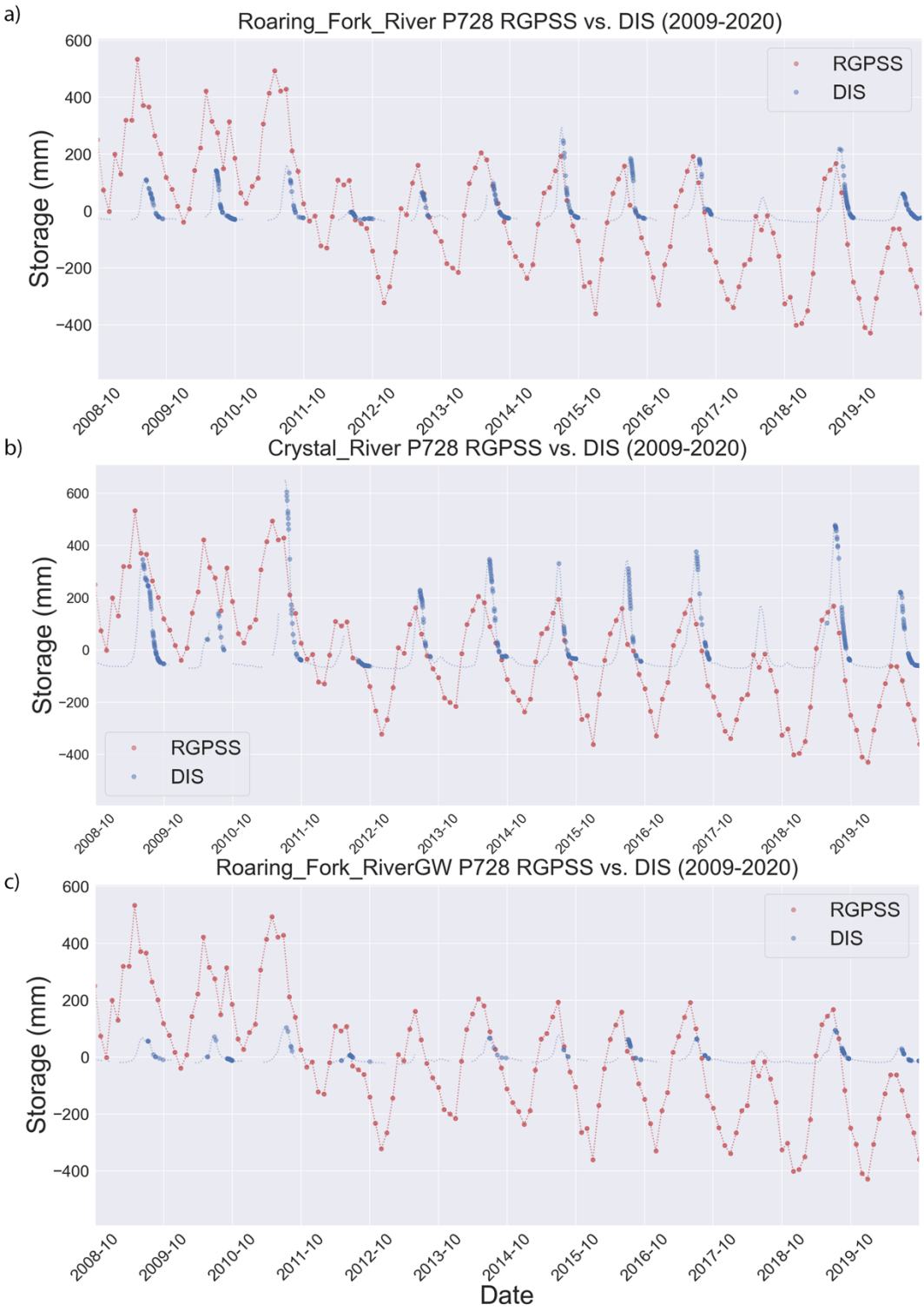

Figure 9.2*: RFRU (a), RFRC (b), and RFRL (c) RGPSS vs. DIS time series comparison of monthly RGPSS (red dots) and 30-day monthly average DIS (blue dots). DIS via Kirchner method is valid only during periods of recession meeting (P,ET <<Q) but blue dotted lines predict DIS for remainder of year and do not include P or ET and are included for reference and for following temporal progression of storage estimates.*

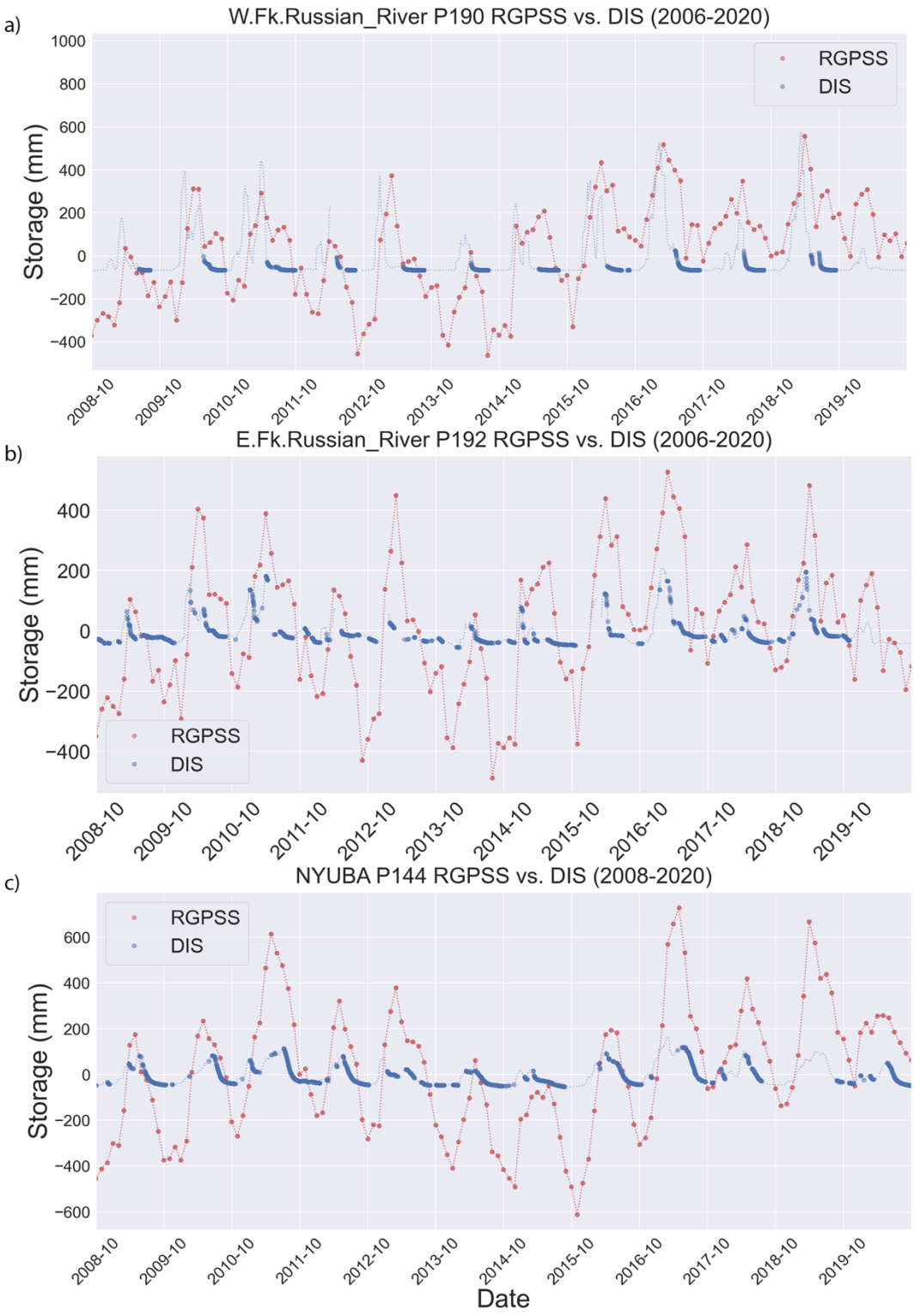

Figure 9.3*: WFRR (a), EFRR (b), and NYUBA (c) RGPSS vs. DIS time series comparison of monthly RGPSS (red dots) and 30-day monthly average DIS (blue dots). DIS via Kirchner method is valid only during periods of recession meeting (P,ET <<Q) but blue dotted lines predict DIS for remainder of year and do not include P or ET and are included for reference and for following temporal progression of storage estimates.*

***Table 2**: R^2 metrics for monthly RGPSS storage correlation comparison to monthly GPSVD, monthly discharge(Q), and DIS for each watershed/GPS site:*

GPS site	RGPSS : Q	recession RGPSS : Q	GPSVD(30) : Q	recession GPSVD(30) : Q	recession RGPSS : DIS	recession: GPSVD(30) : DIS	GPSVD(30) : RGPSS
EFRR	0.44	0.261	0.24	0.17	0.21	0.17	0.6
WFRR	0.29	0.17	0.19	0.22	0.16	0.21	0.3
NYUBA	0.52	0.54	0.52	0.67	0.56	0.63	0.7
CC P350	0.25	0.27	0.27	0.32	0.27	0.32	0.4
CC P019	0.15	0.09	0.27	0.48	0.09	0.47	0.01
RFRC	0.11	0.3	0.05	0.5	0.31	0.51	0.08
RFRU	0.09	0.2	0.05	0.51	0.21	0.53	0.13
RFRL	0.12	0.36	0.03	0.54	0.38	0.57	0.12

4. Discussion

Hysteretic Behavior

GPSVD-Q relationships show reproduceable seasonal patterns, which we interpret as seasonal changes in the storage-discharge relationship. Similar seasonal patterns appear to emerge in all study watersheds according to watershed type. Hysteresis loop temporal progression with 30-day smoothing offers a qualitative classification between our snow-dominated (counter-clockwise temporal progression) (Figure 4: a, b, c, d, and e), rain-dominated (clockwise temporal progression) (Figure 4: f and g), and transitional (approximately linear temporal progression) (Figure 4h) watersheds.

All snow-dominated watersheds (Figure 4: a, b, c, d, and e) display a distinct period of GPSVD downward movement, without significant changes in discharge, coinciding with months associated with snowpack accumulation. We interpret these nearly horizontal lines to indicate relative duration of seasonal snow accumulation and relative importance of snowpack contribution to storage in each watershed. Watersheds experiencing larger total displacement during observed horizontal shifts (ie., vertical displacements) in GPSVD indicate greater snowpack accumulation as observed in RFR relative to CC (Figure 4: a, b, c, d, and e). Snowpack accumulation begins in late November in both RFR and CC however, the duration of snow accumulation in RFR is greater (> 1 month). Relative storage additions from snowpack accumulation, on average, can be assessed from differences in total average annual GPSVD and the GPSVD negative displacement during the winter snow accumulation interval. For example (Figure 4 c, d, and e), total annual GPSVD in RFR is ~16 mm. Yet, during months of snowpack accumulation, the negative vertical displacement in GPSVD is ~10 mm indicating that roughly 63% of annual storage occurs in winter months. In CC P350 (Figure 4 b), total annual GPSVD is ~18 mm with ~10 mm of downward GPSVD associated with snowpack indicating 56% of annual storage associated with GPSVD under hydrologic loading occurs in winter months.

Melt season duration and relationship analysis offers insights into the average hydrologic response of a watershed to seasonal climate conditions. In CC (Figure 4: a and b) discharge increases without significant change to GPSVD until approaching peak discharge. We interpret the minimal movement in GPSVD as reconnection of terrestrial and stream-connected storage.. During this period terrestrial storage in the form of springtime precipitation, infiltration, and

recharge as snowpack melts rapidly reconnect to the stream and no significant changes in storage are observed as discharge increases. One might expect a slight decrease in GPSVD during this interval. We attribute this lack of movement in GPSVD to reflect the ability of local tributaries and streams to distribute excess discharge from higher elevations to other down-gradient recharge zones within the watershed. In RFR watersheds however (Figure 4: c, d, and e), GPSVD begins to rebound midway through the melt season period. This may indicate losses of storage due to sublimation and ET at RFR's higher elevations (> 1000 m) as temperatures increase during this period in the semi-arid Rocky Mountains.

Hysteretic behavior displayed in GPSVD-discharge relationships in our studies rain-dominant watersheds appears to be approximately linear over the entire water year. Adjacent sub-watersheds in the upper Russian River, WFRR and EFRR (Figure 4: f and g), are roughly the same size (~250 km^2) and display similar total annual GPSVD (~13 mm). However, WFRR experiences differences in discharge >3 orders of magnitude compared to EFRR. We attribute the lower variability in discharge in the EFRR to cross-basin inputs diverted from the Eel River that maintain discharge despite agricultural withdrawals in the Potter Valley. This diversion skews natural storage-discharge relationships. Proximity of Lake Mendocino to WFRR and EFRR GPS stations, P190 (~2 km) and P192 (~11 km), likely affect GPSVD as a proxy for storage in these sub-watersheds, artificially decreasing GPSVD (downward displacement) in both. This may explain the poor agreement in R^2 values for raw daily values in WFRR and EFRR ($R^2 < 0.1$), even with 30-day smoothing. We anticipate R^2 values would improve here if GPSVD associated with Lake Mendocino storage was accounted for and removed.

NYUBA is the only transitional watershed investigated in this study. At every level of smoothing, NYUBA displays the strongest linearity in GPSVD-discharge relationship relative to all other watersheds investigated. This linearity is visually apparent in the 30-day hysteresis plots (Figure 3h) and the strength of the relationship is reflected in R^2 values from both daily values and recession periods, $R^2 = 0.45$ and 0.62, respectively (Figure 8.1 or Table 1). Average daily behavior of GPSVD-Q in NYUBA over the period of record and hydrograph recession periods show even stronger relationships ($R^2 = 0.92$ and 0.96, respectively) (Figure 8.1 or Table 1). October through April (Figure 4h) display more variability in linearity in the GPSVD-discharge relationship as these are the "wet months" that deliver the majority of precipitation to NYUBA. Snow accumulation occurs briefly here and is noticeable in the slight horizontal shift in GPSVD in late January and February exhibiting the brief transition from rain to snow dominant watershed characteristics. Hydrograph recession occurs May-September displaying relatively stronger linearity in GPSVD-Q relationship. NYUBA is a transitional watershed but is located at mid-elevations in the Sierra Nevada Mountain Range and thus snow accumulation is brief (< 1 month). We interpret NYUBA to display a linear GPSVD-discharge relationship consistent with a rain-dominated watershed not affected by anthropogenic activities such as diversions or reservoirs.

Using GPSVD, seasonal differences could provide insight into ET measurements. For instance, total annual GPSVD in RFR (Figure 4: c, d, and e) is ~16 mm, on average. Yet, during hydrograph recession, GPSVD rebounds only ~10 mm leaving a remainder of ~6 mm. Rebound not accounted for by discharge is potentially storage lost to sublimation, ET, or groundwater export. CC P350 (Figure 4 b), displays a brief period of similar behavior in April, but is less noticeable with GPSVD showing < 4 mm rebound. Attempts to tease out ET indicators from GPSVD-discharge relationships are not easily observable in rain-dominated or transitional watersheds in this study when investigating POR average behavior. As ET is spatially and

temporally variable, individual water year analysis of GPSVD-discharge relationships, in conjunction with meteorological data, may prove more insightful and should be further investigated.

GPSVD-Q relationship plots form hysteresis loops where distinct seasonal loading patterns emerge between snow-dominated and rain-dominated/transitional watersheds. These reproducible patterns provide insight into seasonality in storage and transport unique to each watershed. GPSVD-Q relationships provide hydrologists and water resource management a new tool with increased spatial and temporal resolution offering independent insight into watershed function at local to intermediate scales.

GPSVD-Q relationship analysis:

In most of our study watersheds, there is no strong linear relationship displayed in GPSVD-Q when analyzing raw, unsmoothed daily values (Figure 8.1 and Table 1). This lack of agreement is reasonable for analysis over the full time series, as we wouldn't expect a strong relationship during seasonal periods where storage and discharge aren't fully coupled (i.e., snowpack accumulation or periods with high ET). We expected GPSVD to be highly correlated during periods of hydrograph recession (and P,ET<<Q) when discharge is assumed to be responding approximately linearly to storage (e.g., Brutsaert and Nieber, 1977; Kirchner, 2009), making $\frac{dS}{dt} = -Q$ in (equation 1). The caveat here is completely accounting for ET, which remains elusive since we are limited to daily averages due to GPSVD daily averages.

During hydrograph recession all watersheds display a similar response, and GPSVD appears to be rebounding at an approximately linear rate (Figures 2.1-2.3, 3.1-3.3, and 4) in response to storage loss through discharge, which is decreasing at an approximately linear rate. Indeed, R^2 values were greatly improved during hydrograph recession periods indicating that the GPSVD-discharge relationship may offer important information on storage at daily to monthly resolution during these periods critical to water users in the arid western United States.

Strong correlations are found when analyzing the average behavior over the period of record between GPSVD-discharge and GPSVD-DIS relationship in most watersheds, excluding RFR watersheds (Figure 8.1 and Table 1). Investigating average daily values over the period of record (POR) during hydrograph recession, we find GPSVD and discharge, as well as GPSVD and DIS (Figure 8.2 and Table 1), to be well correlated in all watersheds indicating the average response of GPSVD to changes in discharge provide important information about local changes in watershed storage and insight into the storage-discharge relationship.

We interpret the upward rebound displayed by GPSVD during hydrograph recession periods to be most sensitive to local scale storage losses exiting the watershed as discharge. Hydrograph recession periods show discharge and GPSVD are strongly correlated, especially when analyzing average POR behavior with 30-day smoothing (R^2 = 0.78 to 0.96) (Figure 8.1 and Table 1). As discharge decreases, GPSVD rebounds and the GPSVD-discharge relationship appears approximately linear in all watersheds (Figures 2.1 – 2.3). This relationship is most obvious from mid-hydrograph recession to baseflow periods when stream flows are primarily maintained from stream-connected storage (e.g., Riegger and Tourian, 2014) when effects from precipitation and ET are minimized (Kirchner, 2009).

At all sites (Figure 5.1 - 5.3) isolated hydrograph recession period GPSVD-Q relationships display an approximately linear relationship that mimic power law functions (Equation 4) we expect to find in storage-discharge relationships (Kirchner, 2009). This behavior

is subdued in RFR watersheds, which show strong linearity through the end of the water year (Sep.30th). RFR watersheds continue baseflow recession through the winter while simultaneously building storage as snowpack, thus exhibiting the nearly straight line but discharge continues its recession through spring (Figures 2.2 and Figure 4 c, d, and e). The similarity of GPSVD-Q to storage-discharge relationships provides qualitative evidence, and high R^2 values provide quantitative evidence, that further strengthen our assertion that local GPSVD can be used as a proxy for storage at local to intermediate watershed scales. This indicates that GPSVD-discharge relationships may be employed further to infer storage and thus, water availability during hydrograph recession periods most important to water resource users and management and should be further investigated.

Curvature changes in GPSVD-discharge relationships for individual years (in blue), exemplified at CC's mountainous, high elevation GPS site (P350) (Figure 5.1 b) indicate GPSVD-discharge relationship differences potentially based on local antecedent conditions and climate effects. Interannual hydrograph recession periods displaying horizontal shifts left of average behavior (red) likely indicate increased hydrologic loading due to increased storage in the system; and shifts right of the average behavior would indicate less storage present at the onset of hydrograph recession periods. These observations indicate that interannual differences in GPSVD-discharge relationships are more sensitive to antecedent conditions relative to annual precipitation accumulation. This further agrees with storage-discharge theory (Kirchner, 2009) where more storage results in increased discharge rates and less storage results in decreased discharge rates. The observed horizontal shifts in interannual behavior as described by GPSVD may expose a shortcoming when assessing relationships or making predictions using the average behavior over the period of record. These interannual anomalies are important and may provide key insights into how the GPSVD-DIS and GPSVD-Q relationships change under different antecedent or changing climatic conditions and should be further investigated for potential employment to assess watershed sensitivity to changes in climate.

Greater variability in GPSVD-discharge relationships from snow-dominant, high elevation GPS station locations (Figures 5.1 b and 5.2 a and b) suggest that high elevation GPS sites are more sensitive to changes in storage and/or antecedent conditions or that high elevations see the largest changes in storage interannually. Although precipitation is both spatially and temporally variable, these sites typically accumulate the most precipitation and suffer greater losses to sublimation, ET, and downgradient transport as water moves toward watershed outlets relative to lower elevation GPS site locations. Higher elevation sites would also be expected to have more available subsurface storage, with larger unsaturated zones. This is exemplified in CC with high elevation site P350 (Figure 5.1 b) and mid-elevation site P019 (Figure 5.1 a). The lower elevation site P019 displays much less variability in relationship slope changes and horizontal shifts. This makes sense as mid-elevation GPS sites should maintain storage longer relative to high elevation sites as subsurface groundwater is transported downgradient through the mountain block to lower elevations.

At the upper end of hydrograph recession, when discharge is near peaks and GPSVD is lowest, rain-dominant watersheds WFRR and EFRR (Figure 5.3: a and b) display large variability in relationship scatter plots. But like all other watersheds, the relationship strengthens during the period from mid-hydrograph recession to the end of the water year. This is expected as precipitation decreases and ET is minimized during these periods when less soil moisture is available to be lost to ET (eg., Woodward, 1987; Neilson, 1995).

The strong agreement found in average GPSVD-discharge relationships provide convincing evidence that GPSVD is providing important information on storage at local to intermediate watershed scales, arguably most important during hydrograph recession periods most critical to hydrologist and water resources management.

RGPSS-discharge, RGPSS-DIS, and GPSVD relationships:

A major purpose of this study was to test if GPSVD could provide a proxy for storage or improved information on storage at local to intermediate watershed scales. We have shown both qualitative and quantitative evidence that GPSVD is a proxy for storage, especially during hydrograph recession periods when storage losses have the strongest relationship to discharge (e.g., Brutsaert and Nieber, 1977; Kirchner, 2009). We further tested this assumption by analyzing relationships between RGPSS and discharge, GPSVD, and DIS. For this analysis, we used monthly RGPSS storage values and compared them to 30-day weighted average values on the last day of each month for discharge, GPSVD, and DIS. We compared the RGPSS estimate using the pixel closest to each GPS station, which is weighted toward the local site but incorporates all (>1500) GPS stations across the western U.S. to provide a change in storage estimates (Argus, et al. 2017). One caveat here is that RGPSS storage estimates are different in that they account for large reservoirs by removing associated vertical displacements from the vertical GPS signal whereas the GPSVD analysis does not remove effects of associated local hydrologic loading. We also acknowledge the difference in both spatial and temporal resolution between RGPSS (regional scale) and DIS (local watershed scale) may adversely affect results, especially given the temporal constraints of hydrograph recession periods where DIS meets the criteria of P, ET<< Q (~2.5 to 4+ months) thus, further limiting data points for analysis at monthly resolution over short hydrograph recession periods.

First, we compare RGPSS-Q and GPSVD-Q relationships to see how GPSVD, as a proxy for storage, compares to regional storage inferences from RGPSS during hydrograph recession periods. The close agreement in relationships (R^2 < +/- 0.2) indicate that local GPSVD is providing information on storage (Table 2). This makes sense as the RGPSS storage estimates from inversion are weighted to nearby GPS stations. Exceptions are in CC P019, WFRR, EFRR, and NUBA which exhibit significant increases in R^2 values gaining (+0.18 to +0.39) comparing GPSVD-Q relative to RGPSS-Q indicating that GPSVD-Q relationships are stronger in these watersheds. Perhaps the difference in agreement comes from array density as RFR watersheds have few GPS stations in proximity and RGPSS is more reliable with increased GPS array density (eg., Argus et al., 2017). However, CC P019 is proximal to CC P350 and in the same watershed yet, displays a significantly larger gain in R^2 values using GPSVD (+0.39). We would expect better agreement between RGPSS-Q and GPSVD-Q relationships at CC P019 due to its proximity to CC P350 as both sites occupy the same watershed and have identical hydrograph recession periods.

We compared the two independent inferences of storage, RGPSS and DIS, to assess agreement with each other (Table 2). We found weak agreement between the two storage inferences in all watersheds except NYUBA which displays moderate agreement (R^2 = 0.56). We expected to find better agreement in all watersheds where RGPSS-Q and GPSVD-Q showed moderate relationships (EFRR, WFRR, and P350) and lean on spatial and temporal caveats listed above as to why they do not.

Given the overall poor agreement found in RGPSS-DIS, we wanted to see how they compared to GPSVD-DIS relationships. Relative to RGPSS-DIS, all sites display increased R^2 values (+0.05 to +0.37) for GPSVD-DIS relationships during hydrograph recession periods except for EFRR (-0.08). Again, we see gains in R^2 values ranging from (+0.18 to +0.37) with the largest increase in R^2 value (+0.37) in CC P019. These results are not surprising as DIS is derived from discharge and are expected to be like those found when comparing RGPSS and GPSVD to discharge.

Our comparisons between regional (RGPSS) and local inferences of storage (GPSVD) indicate that GPSVD-DIS and GPSVD-RGPSS are in close agreement in the transitional (NYUBA) and rain-dominated (WFRR and EFRR) watersheds. Conversely, in sparsely GPS instrumented snow-dominated watersheds (CC and RFR), local GPSVD is more representative of local storage relative to RGPSS. The main difference between rain-dominant and snow-dominant study sites in this study is decreased density of GPS sites at our snow dominated locations and perhaps highlights the ability of RGPSS with adequate GPS coverage. CC P350 is an example of a snow-dominant watershed that shows agreement between both relationships and again, this may be due to the proximity of the GPS station to regional NOTA GPS array and decreased GPS instrumentation density. EFRR stands out as having a stronger relationship to RGPSS inferences and this may be due to RGPSS's removal of the local reservoir (Lake Mendocino) and/or diversion additions from the Eel River, which neither are accounted for in our local GPSVD analysis. Our observations indicate that in local to intermediate watersheds with decreased GPS station density, the local GPSVD appears to be a better indicator of storage than RGPSS.

5. Conclusions

Strong correlations between GPSVD and discharge and DIS suggest that the GPSVD-discharge relationship has valuable information on watershed storage at local watershed scales, especially during hydrograph recession periods when storage losses are primarily attributed to discharge (e.g., Brutsaert and Nieber, 1977; Kirchner, 2009). Like Bevis et al. (2005), our results indicate that GPSVD responds by moving downward under hydrologic loading and rebounds as these loads are removed. GPSVD responds to individual hydrologic processes (i.e., snowpack or precipitation accumulation). We observe that GPSVD maximums consistently occur during minimum discharge and align with water year boundaries when storage and discharge are expected to be at annual minimums. Observations of elastic surface displacement in response seasonal hydrologic loading demonstrate that GPSVD is indicative of changes in annual storage at local scales.

Over the period of record, average daily GPSVD-discharge values are well correlated during hydrograph recession periods at small to intermediate watershed scales when smoothed daily to monthly, showing R^2 values (0.20 to 0.91) and (0.78 to 0.96), respectively. We compared monthly averages of DIS to monthly averaged inferred storage from RGPSS and find agreement between the two storage inferences in transitional and rain-dominated watersheds proximal to dense portions of the regional GPS array network. GPSVD-DIS showed improved relationships in snowpack-dominated, less dense GPS array network areas and displayed a moderate relationship (R^2 = 0.46 to 0.56) in these areas relative to RGPSS. The agreement between GPSVD-DIS and RGPSS-DIS relationship found provides evidence that local GPSVD is providing information at local to intermediate watershed scales on par with current regional GPS published methods. And the improved relationships of GPSVD-DIS vs. RGPSS-DIS where

GPS array density is lacking highlights the potential of GPSVD as a proxy measurement of local watershed storage and can perhaps offer improved spatial and temporal resolution relative to current published RGPSS methods to estimate storage at local watershed scales. The GPSVD-discharge relationship offers unprecedented insights into watershed functions of storage and transport across a variety of different watersheds and can enhance predictive power when estimating water availability at local to intermediate watershed scales most important to hydrologist and water resources management.

Acknowledgements

This material is based upon work supported by the National Science Foundation under grants EAR-1900646 and 2021637. I would like to thank Dr. Ellen Knappe for her expertise and guidance regarding geodetic signal acquisition and processing, as well as her overall support over the duration of this study.

References

Abatzoglou, J.T., 2013, Development of gridded surface meteorological data for ecological applications and modelling: International Journal of Climatology, v. 33, p. 121-131, doi: 10.1002/joc.3413.

Argus, D., 2014, Seasonal variation in total water storage in California: Geophysical ResearchLetters, p. 6413–6419, doi:10.1002/2014GL061184.

Argus, D.F., Landerer, F.W., Wiese, D.N., Martens, H.R., Fu, Y., Famiglietti, J.S., Thomas, B.F., Farr, T.G., Moore, A.W., and Watkins, M.M., 2017, Sustained Water Loss in California's Mountain Ranges During Severe Drought From 2012 to 2015 Inferred From GPS: Journal of Geophysical Research: Solid Earth, v. 122, p. 10,559-10,585, doi:10.1002/2017JB014424.

Barnett, T.P., Adam, J.C., and Lettenmaier, D.P., 2005, Potential impacts of a warming climate on water availability in snow-dominated regions: Nature, v. 438, p. 303-309, doi: 10.1038/nature04141.

Berghuijs, W.R., Hartmann, A., and Woods, R.A., 2016, Streamflow sensitivity to water storage changes across Europe: Geophysical Research Letters, v. 43, p. 1980–1987, doi:10.1002/2016GL067927.

Bevis, M., Alsdorf, D., Kendrick, E., Luiz, P.F., Forsberg, B., Robert, S.,Jr, and Becker, J., 2005, Seasonal fluctuations in the mass of the Amazon River system and Earth's elastic response: Geophysical Research Letters, v. 32, p. L16308-n/a, doi: 10.1029/2005GL023491.

Birhanu, Y., and Bendick, R., 2015, Monsoonal loading in Ethiopia and Eritrea from vertical GPS displacement time series: Journal of Geophysical Research.Solid Earth, v. 120, p. 7231-7238, doi: 10.1002/2015JB012072.

Borsa, A. A., Agnew, D. C., & Cayan, D. R. (2014). Ongoing drought-induced uplift of the western United States. *Science*, 345(6204), 1587– 1590. https://doi-org.weblib.lib.umt.edu:2443/10.1126/science.1260279

Botter, G., Porporato, A., Rodriguez-Iturbe, I., and Rinaldo, A., 2009, Nonlinear storage-discharge relations and catchment streamflow regimes: Water Resources Research, v. 45, p. 1–16, doi:10.1029/2008WR007658.

Brutsaert, W., Nieber, J.L., 1977. Regionalized drought flow hydrographs from a mature glaciated plateau. Water Resour. Res. 3 (3), 637–643.

Brutsaert, W., Lopez, J.P., 1998. Basin-scale geohydrologic drought flow features of riparian aquifers in the southern great plains. Water Resour. Res. 34 (2), 233–24.

Dill, R. and H. Dobslaw (2013), Numerical simulations of global-scale high-resolution hydrological crustal deformations,
J. Geophys. Res. Solid earth 118, doi:10.1002/jgrb.50353.

Donat, Markus, Andrew Lowry, Lisa Alexander, Paul O'gorman, and Nicola Maher. "More Extreme Precipitation in the World's Dry and Wet Regions." Nature Climate Change 6.5 (2016): 508-13.

Dong, D., P. Fang, Y. Bock, M. K. Cheng, and S. Miyazaki. "Anatomy of Apparent Seasonal Variations from GPS-derived Site Position Time Series." Journal of Geophysical Research: Solid Earth 107.B4 (2002): ETG 9-1-TG 9-16. Web.

Earman, S., Campbell, A.R., Phillips, F.M., and Newman, B.D., 2006, Isotopic exchange between snow and atmospheric water vapor: Estimation of the snowmelt component of groundwater recharge in the southwestern United States: Journal of Geophysical Research.Atmospheres, v. 111, , doi: 10.1029/2005JD006470.

Farrell, W.E., 1972, Deformation of the Earth by surface loads: Reviews of Geophysics, v. 10, p. 761–797, doi:10.1029/RG010i003p00761.

Fu, Y., Argus, D. F., & Landerer, F. W. (2015). Seasonal and interannual variations of water storage in Washington and Oregon estimated from GPS measured surface loading deformation. *Journal of Geophysical Research: Solid Earth*, 120, 552– 566. https://doi-org.weblib.lib.umt.edu:2443/10.1002/2014JB011415

Heki, K., 2001, Seasonal modulation of interseismic strain buildup in northeastern Japan driven by snow loads: Science, v. 293, p. 89–92, doi:10.1126/science.1061056.

Herring, T. A., T. I. Melbourne, M. H. Murray, M. A. Floyd, W. M. Szeliga, R. W. King, D. A. Phillips, C. M. Puskas, M. Santillan, and L. Wang (2016), Plate Boundary Observatory and related networks: GPS data analysis methods and geodetic products, Rev. Geophys., 54, doi:10.1002/2016RG000529.

Horton, R. E. (1936), Natural stream channel-storage, EosTrans. AGU, 17, 406.

Horton, R. E. (1937), Natural stream channel-storage (second paper), Eos Trans. AGU, 18, 440.

Horton, R. E. (1941), Virtual channel-inflow graphs, Eos Trans. AGU, 22, 811.

Kirchner, J.W., 2009, Catchments as simple dynamical systems: Catchment characterization, rainfall-runoff modeling, and doing hydrology backward: Water Resources Research, v. 45, p. 1–34, doi:10.1029/2008WR006912.

Klos, A., Bogusz, J., Figurski, M., and Kosek, W., 2016, On the Handling of Outliers in the GNSS Time Series by Means of the Noise and Probability Analysis BT - IAG 150 Years, *in* Rizos, C. and Willis, P. eds., Cham, Springer International Publishing, p. 657–664.

Knappe, E., Bendick, R., Martens, H.R., Argus, D.F., and Gardner, W.P., 2019, Downscaling Vertical GPS Observations to Derive Watershed-Scale Hydrologic Loading in the Northern Rockies: Water Resources Research, v. 55, p. 391–401, doi:10.1029/2018WR023289.

Martens, H.R., Simons, M., Owen, S., and Rivera, L., 2016, Observations of ocean tidal load response in South America from subdaily GPS positions: Geophysical Journal International, v. 205, p. 1637-1664, doi: 10.1093/gji/ggw087.

Maxwell, Reed M, Laura E Condon, Stefan J Kollet, Kate Maher, Roy Haggerty, and Mary Michael Forrester. "The Imprint of Climate and Geology on the Residence times of Groundwater." Geophysical Research Letters 43.2 (2016): 701-08.

Meixner, T., Manning, A. H., Stonestrom, D. A., Allen, D. M., Ajami, H., Blasch, K. W., . . . Walvoord, M. A. (2016). Implications of projected climate change for groundwater recharge in the western united states. *Journal of Hydrology, 534*, 124-138. doi:10.1016/j.jhydrol.2015.12.027

Neilson, R.P.., F., 1995, A model for predicting continental-scale vegetation distribution and water balance: Ecological Applications, v. 5, p. 362-385, doi: 10.2307/1942028.

Ouellette, K.J., de Linage, C., and Famiglietti, J.S., 2013, Estimating snow water equivalent from GPS vertical site-position observations in the western United States: Water Resources Research, v. 49, p. 2508–2518, doi:10.1002/wrcr.20173.

Riegger, J., and M. J. Tourian. "Characterization of Runoff-storage Relationships by Satellite Gravimetry and Remote Sensing." Water Resources Research 50.4 (2014): 3444-466.

Steckler, Michael S., Scott L. Nooner, S. Humayun Akhter, Sazedul K. Chowdhury, Srinivas Bettadpur, Leonardo Seeber, and Mikhail G. Kogan. "Modeling Earth Deformation from Monsoonal Flooding in Bangladesh Using Hydrographic, GPS, and Gravity Recovery and

Climate Experiment (GRACE) Data." Journal of Geophysical Research: Solid Earth 115.B8 (2010): N/a.

Tromp-Van Meerveld, H.J., and McDonnell, J.J., 2006, Threshold relations in subsurface stormflow: 1. A 147-storm analysis of the Panola hillslope: Water Resources Research, v. 42, p. 1–11, doi:10.1029/2004WR003778.

van Dam, T., Blewitt, G., Larson, K.M., Lavalee, D., Milly, P.C.D., Shmakin, A.B., and Wahr, J.M., 2001, Crustal displacements due to continental water loading: Geophysical Research Letters, v. 28, p. 651–654

Wang, H., Xiang, L., Jia, L., Jiang, L., Wang, Z., Hu, B., & Gao, P. (2012). Load Love numbers and Green's functions for elastic Earth models PREM, iasp91, ak135, and modified models with refined crustal structure from crust 2.0. *Computational Geosciences*, 49, 190– 199. https://doi-org.weblib.lib.umt.edu:2443/10.1016/j.cageo.2012.06.022

Woodward, F.I., 1987, Climate and plant distribution: Cambridge Cambridgeshire]; New York, Cambridge Cambridgeshire; New York : Cambridge University Press, .

Yager, R.M., 2018, Characterization and occurrence of confined and unconfined aquifers in quaternary sediments in the glaciated conterminous United States: https://doi.org/10.3133/sir20185091.